Redox Biology 63 (2023) 102714

Contents lists available at ScienceDirect

Redox Biology

journal homepage: www.elsevier.com/locate/redox

LPS-induced mitochondrial dysfunction regulates innate immunity activation and α-synuclein oligomerization in Parkinson's disease

A. Raquel Esteves [a,b,c,1], Diana F. Silva [a,b,c,1], Diogo Banha [a,c], Emanuel Candeias [a,b,c], Beatriz Guedes [a,c], Sandra M. Cardoso [a,c,d,*]

[a] CNC–Center for Neuroscience and Cell Biology, University of Coimbra, Coimbra, Portugal
[b] IIIUC-Institute for Interdisciplinary Research, University of Coimbra, Coimbra, Portugal
[c] Center for Innovative Biomedicine and Biotechnology, University of Coimbra, Coimbra, Portugal
[d] Institute of Biology, Faculty of Medicine, University of Coimbra, Coimbra, Portugal

ARTICLE INFO

Keywords:
Parkinson's disease
Lipopolysaccharides
Mitochondrial dysfunction
Innate immunity activation
α-synuclein oligomerization

ABSTRACT

Sporadic Parkinson's disease (sPD) is a complex multifactorial disorder which etiology remains elusive. Several mechanisms have been described to contribute to PD development namely mitochondrial dysfunction, activation of inflammatory pathways and the deposition of unfolded proteins such as α-synuclein. Our work shows for the first time that lipopolysaccharide (LPS)-induced activation of innate immunity requires a functional mitochondria and mimics PD pathology in cells. We found in primary mesencephalic neurons that LPS targeted the mitochondria and activated neuronal innate immune responses, which culminated with α-synuclein oligomerization. Moreover, in cybrid cell lines repopulated with mtDNA from sPD subjects with inherent mitochondrial dysfunction and NT2-Rho0 obtained by long-term ethidium bromide exposure, and so without a functional mitochondrial, LPS was not able to further activate innate immunity or increase α-synuclein aggregation.

Herein, we showed that mesencephalic neurons are able to activate innate immunity after LPS exposure and this pathway is dependent on mitochondria. Moreover, we disclose that α-synuclein over production is an innate immune response. Our data indicate that mitochondria provide the base for innate immunity activation in idiopathic PD.

1. Introduction

Sporadic Parkinson's disease (sPD) is a complex, multifactorial neurodegenerative disease and its etiology remains a matter of debate. PD is the second most common neurodegenerative disease and is characterized by the selective loss of dopaminergic neurons. Although the cause of death of dopamine (DA)-secreting neurons is still elusive, oxidative stress originated from mitochondrial impairment have been proposed to contribute to PD pathogenesis [1]. Two main hypothesis have been proposed to explain the etiology of sPD: one is based on the notion that oligomeric α-synuclein (a-syn), the main constituent of Lewy bodies (LBs) [2], is toxic [3] and may contribute to the death of Substantia Nigra Pars Compacta (SNpc) DA neurons. An alternative hypothesis is that the loss of SNpc DA neurons in PD is driven by mitochondrial dysfunction [4,5]. The identification of mutations in the *PINK1* and *PARKIN* genes causing familial PD [6] provide major evidence on the role of mitochondrial influence in PD pathogenesis [7]. These two hypotheses are complementary rather than conflicting, since a-syn was shown to selectively localize within mitochondrial sub-compartments upon certain stimuli [8], which results in mitochondrial malfunctioning. Interestingly, it has been pointed that bacterial and viral pathogen infections are associated with a higher risk for developing PD [9] and that a-syn might be produced as part of an immune response acting as an antimicrobial peptide (AMP), exhibiting antibacterial and antifungal activities [10]. Additionally, neuroinflammation, is considered an aggravator factor in PD neurodegenerative process resulting in the activation of microglia cells with deleterious effect on neurons because of the production of pro-inflammatory cytokines [9,11]. It was found in *postmortem* samples of striatum and in cerebrospinal fluid of PD subjects, that the levels of various cytokines are significantly increased, namely tumor necrosis

* Corresponding author. CNC - Center for Neuroscience and Cell Biology, University of Coimbra, Largo Marquês de Pombal, 3004-517, Coimbra, Portugal.
E-mail addresses: esteves.raquel@gmail.com (A.R. Esteves), dianaffsilva@gmail.com (D.F. Silva), banhadiogo@hotmail.com (D. Banha), beaatrizguedes@gmail.com (B. Guedes), sicardoso@fmed.uc.pt, cardoso.sandra.m@gmail.com (S.M. Cardoso).
[1] Authors contributed equally to this work.

https://doi.org/10.1016/j.redox.2023.102714
Received 27 March 2023; Received in revised form 23 April 2023; Accepted 23 April 2023
Available online 25 April 2023

Abbreviations:

sPD	Sporadic Parkinson's disease
DA	Dopamin
a-syn	α-synuclein
LBs	Lewy Bodies
SNpc	Substantia nigra pars compacta
TNF-α	tumor necrosis factor alpha
IL	Interleukin
DAMPs	damage associated molecular patterns
ROS	reactive oxygen species
mtDNA	mitochondrial DNA
sPD cybrids	sporadic Parkinson's disease cybrids
LPS	Lipopolysaccharide
NLRP3	nucleotide-binding domain, leucine-rich–containing family, pyrin domain–containing-3
TLR	Toll-like Receptor
PRR	Pattern Recognition Receptor
OCR	Oxygen consumption rate
HBSS	Hanks' balanced salt solution
PAMPs	pathogen associated molecular patterns

factor (TNF)-α, interleukin (IL)-1β, IL-2; IL-4 and IL-6. Previous results show that neurons can also mount innate immune responses [12,13] after pathogen infection or exhibition of damage associated molecular patterns (DAMPs) [14,15]. Upon mitochondrial damage, DAMPs can stimulate the overproduction of reactive oxygen species (ROS). ROS promotes mitochondrial transition pore opening, favoring mitochondrial uncoupling and further increasing ROS generation in a feed-forward circuitry. After pore opening, the release of mitochondrial DNA (mtDNA) into the cytosol and cardiolipin exposure to the mitochondrial outer membrane, stimulate activation of the nucleotide-binding domain, leucine-rich–containing family, pyrin domain–containing-3 (NLRP3) inflammasome and the production of IL-1β and IL-18 [16].

Bacterial toxins and its effects on mitochondria are assuming greater importance in the progression of sPD as it is hypothesized that the exposure to environmental toxins may be a causative factor for PD, facilitated by individual genetic susceptibility and aging. Here we show that LPS, a bacterial endotoxin, induces mitochondrial dysfunction promoting activation of innate immunity which will lead to the accumulation of a-syn oligomers in enriched mesencephalic neuronal cultures. Moreover, we used complementary cellular models to prove that mitochondrial function is a requisite for innate immunity activation. We show that in cells harboring PD patient mitochondria (sPD cybrids) with basal mitochondrial deficits innate immunity response is already activated promoting a-syn oligomers buildup. In addition, sPD cybrids challenged with LPS failed to induce further damage. Most interestingly, in NT2-Rho0 cells, that lack functional mitochondria due to long term ethidium bromide exposure, LPS did not succeed to induce mitochondrial defects and activate innate immunity traits. Taking these data into account, we propose that mitochondria are the sentinels of the cell, and that functional mitochondria are a requisite for innate immunity activation in sPD.

2. Materials and methods

Chemicals	Manufacturer
5-Fluoro-2′-deoxyuridine (FDU)	Sigma Chemical Co (St. Louis, MO, USA); Cat. No. F0503
Ammonium chloride (NH_4Cl)	Sigma Chemical Co (St. Louis, MO, USA); Cat. No. 9434
Amplex® Red	Thermo Fisher Scientific Inc (Waltham, MA USA); Cat. No. A22188
Antimycin	Sigma Chemical Co (St. Louis, MO, USA); Cat. No. A8674
Carbonyl cyanide 4-(trifluoromethoxy) phenylhydrazone (FCCP)	Sigma Chemical Co (St. Louis, MO, USA); Cat. No. C2920
Caspase 1 substrate (Ac-VAD-4-methoxy-2-naphtylamide)	Sigma Chemical Co (St. Louis, MO, USA); Cat. No. SCP0066
Carbonyl cyanide m-chlorophenyl hydrazone (CCCP)	Sigma Chemical Co (St. Louis, MO, USA); Cat. No. C2759
Leupeptin	Sigma Chemical Co (St. Louis, MO, USA); Cat. No. L2023
Lipopolysaccharides from Escherichia coli O26:B6 (LPS)	Sigma Chemical Co (St. Louis, MO, USA; Cat. No. L2654
MitoTracker Green	Invitrogen (Carlsbad, CA, USA); Cat. No. M7502
MitoPY1	Sigma Chemical Co (St. Louis, MO, USA); Cat. No. SML0734
Oligomycin	Alfa Aesar (Karlsruhe, Germany); Cat. No. J60211
Rotenone	Sigma Chemical Co (St. Louis, MO, USA); Cat. No. R8875
Tetramethylrhodamine, methyl ester (TMRM)	Molecular Probes (Eugene, OR, USA); Cat. No. T668
Mowiol 4-88	Sigma Chemical Co (St. Louis, MO, USA); Cat. No. 81381
10-N-Nonyl acridine orange (NAO)	Enzo Lifesciences (Lausen, Switzerland); Cat. No. 08091739
3-(4,5-dimethylthiazol-2-yl) 2,5-diphenyltetrazolium bromide (MTT)	Sigma Chemical Co (St. Louis, MO, USA); Cat. No. M2128

Antibodies	Manufacturer
Rabbit anti-phospho DRP1 (serine 616)	Cell Signaling (Cat. No. 3455s)
Rabbit anti-TOM20	Santa Cruz Biotechnology (Cat. No. sc-11415)
Mouse anti-TLR4	Santa Cruz Biotechnology (Cat. No. sc-293072)
Rabbit anti-TLR3	Abcam (Cat. No. ab84911)
Mouse anti-β3-Tubulin	Cell Signaling (Cat. No. 4466)
Mouse β-actin	Sigma (Cat. No. A5441)
Mouse anti-TATA-Binding-Protein	Merck (Cat. No. MAB3658)
Rabbit anti-α-synuclein,*oligomer specific Syn-33*	Sigma (Cat No. ABN2265)
Mouse anti-SDHA	Abcam (Cat. No. ab137746)
Mouse anti-Lamp1	clone H4A3 from the Developmental
Rabbit anti-LC3B	Cell Signaling (Cat. No. 3868)
Mouse anti-α-tubulin	Sigma (Cat. No. T6199)
Rabbit anti-p62	Sigma (Cat. No. P0067)
Goat anti-rabbit Alexa Fluor 488	Molecular Probes, Life Technologies (Cat. No. A11008)
Goat anti-mouse Alexa Fluor 594	Molecular Probes, Life Technologies (Cat. No. A11005)

ELISA Kits	Manufacturer
IL-1β Quantikine ELISA	R&D Systems (Cat. No. MLB00C)
NFκB p65 Total SimpleStep ELISA Kit	Abcam (Cat. No. ab176648)
α Synuclein oligomer (SNCO α) ELISA Kit	MyBioSource (Cat. No. MBS724099)

2.1. Isolation and treatments of primary mesencephalic cultures

Primary neurons were prepared from mesencephalon of C57Bl/6 mice embryos brains at gestation day 14/15 and cultured as described previously [13]. Briefly, embryos were carefully removed under aseptic conditions and collected in Hanks' balanced salt solution (HBSS) [5.36 mM KCl, 0.44 mM KH2PO4, 137 mM NaCl, 4.16 mM NaHCO3, 0.34 mM NaH2PO4.H2O, 5 mM Glucose, 5.36 mM Sodium Pyruvate, 5.36 mM Hepes, 0.001% Fenol Red, (pH 7.2)] at RT. Brains were then dissected and the ventral mesencephalon excised. The removed ventral mesencephalon tissue was incubated in HBSS solution containing trypsin (0.5 g/L) for 15 min at 37 °C. Tissue digestion was stopped by the addition of trypsin inhibitor (type II-S; 0.75 g/L) in HBSS, followed by a

centrifugation at 140×*g* for 5 min. After washing the pellet once with HBSS, the cells were dissociated mechanically and resuspended in fresh Neurobasal medium supplemented with 2 mM L-glutamine, 2% B-27 supplement, penicillin (100,000 U/L), and streptomycin (100 mg/L) and 1% heat-inactivated FBS. The cells were then seeded on poly-L-lysine (0.1 g/L)-coated dishes. For western blotting analysis, caspase-1 determination and ELISA kits, mesencephalic neurons were seeded on poly-L lysine (0.1 mg/mL) coated six-well plates at a density of 1.3×10^6 cells/mL. For immunocytochemistry analysis, mesencephalic neurons were seeded on poly-L-lysine (0.1 mg/mL)-coated coverslips at a density of 0.6×10^6 cells/mL. For seahorse analysis mesencephalic neurons were seeded on poly-L-lysine (0.1 mg/mL)-coated seahorse microplates at a density of 0.6×10^6 cells/mL. For cardiolipin and live imaging analysis, mesencephalic neurons were seeded on poly-L-lysine (0.1 mg/mL)-coated ibidiTreat μ-Slide 8-well plates from GmbH (Germany) (Cat. No. 80821) at a density of 0.6×10^6 cells/mL. For mitochondrial membrane potential and ROS production measurements using MitoPy probe, mesencephalic neurons were seeded on poly-L lysine (0.1 mg/mL) coated 24-well plates at a density of 1.3×10^6 cells/mL. Cultures were grown at 37 °C in a fully humidified air atmosphere containing 5% CO2. On the 4th day in vitro half the medium was replaced with serum-free medium and incubated with 1:2000 5-Fluoro-2′-deoxyuridine (FDU) to inhibit proliferating glial cells. Half of the medium was changed on the 6th and 8th day to serum-free medium. The presence of glial cells in our cultures was monitored after neuronal differentiation. Our results showed undetectable microglial cells (data not shown). After 14 days in vitro, cultured neurons were treated with 1 μg/mL LPS for 48 h, the higher concentration that did not reduce cell viability determined by the MTT-reduction test (SFig. 1a). For all experimental procedures, controls were performed in the absence of LPS. Where indicated, 20 mM NH_4Cl and/or 20 μM Leupeptine (Sigma, St. Louis, MO, USA) were added for 4 h to the culture medium to assess autophagic flux.

2.2. Human subjects

Sporadic PD patients and healthy individuals were recruited after approval by the University of Kansas School of Medicine Institutional Review Board as described previously [17]. None of the patients had alternative diagnoses, degeneration of related systems, drug-induced parkinsonism, or any other serious medical illness. Enrollment was also contingent on the absence of a diagnosis for another neurodegenerative disease. The control subjects were participants of a longitudinal "normal aging/normal cognition" cohort that is characterized serially by the Brain Aging Project at the University of Kansas School of Medicine. These control subjects have not been diagnosed with a neurodegenerative or pre-neurodegenerative disease condition. The age of the PD subjects who participated in this study was 64 + 12.8 years and for the control subjects was 74.3 + 5.5 years. Each experiment was performed at least 3 times and a minimal of three control (CT cybrids) and three sporadic Parkinson's disease patient-derived cybrid cells lines (sPD cybrids) (each derived from a different individual) were used.

2.3. Isolation of platelets from sporadic PD and age-matched controls

After informed consent was given, sporadic PD and age-matched control subjects underwent a 10-ml phlebotomy using tubes containing acid–citrate–dextrose, as an anticoagulant, to provide the platelets needed for cybrid cell fusions. Approximately 7 mL of blood were added to 5 mL of Histopaque in a 50 mL tube. After a centrifugation of 1000×*g* for 10 min a fraction of plasma containing platelets was aspirated and transferred to another clean tube. Plasma fractions were diluted in S-MEM (Gibco, ThermoFisher Scientific, MA, USA; Cat No. 11380–037) medium and underwent centrifugation of 1700×*g* for 15 min. The resultant platelet pellet was used for fusions with NT2 Rho0 (Rho0) cells.

2.4. PD and control cybrids generation, maintenance, and treatments

Cybrid approach consists on the transfer of sporadic PD or age-matched healthy subjects' platelet containing mitochondria to mtDNA-depleted recipient cells (NT2 Rho0 cells) generating hybrid cell lines (cybrids). The resulting cybrid cell lines express the nuclear genes of the recipient Rho0 cell line and the mitochondrial genes of the platelet donor. NT2 Rho0 cells (Stratagene, La Jolla, CA) with neuronal-like characteristics but lacking intact mtDNA due to long-term exposure to ethidium bromide. These cells are grown in Optimem supplemented with 200 μg/mL sodium pyruvate from Sigma (St. Louis, MO, USA), 100 μg/mL uridine from Sigma (St. Louis, MO, USA), and 1% penicillin-streptomycin solution. Consequently, platelet containing mitochondria from either PD or age-matched control subjects were isolated from individual blood samples and were used to repopulate NT2 Rho0 cells with mtDNA by co-incubation in polyethylenoglycol (PEG) as previously described by our group [18]. The resulting cybrids were grown in Rho0 growth medium, in T75-cm^2 tissue culture flasks for 1 week. Seven days after plating, cells that were not repopulated with platelet mtDNA were removed by withdrawal of pyruvate and uridine from the culture medium and substitution of dialyzed, heat-inactivated fetal calf serum for non-dialyzed, heat-inactivated fetal calf serum. Moreover, "mock fusions" in which NT2 Rho0 cells were not incubated with platelets were plated and maintained in the selection medium in parallel with the actual fusions. During the selection period, all cells from the mock fusions died. After selection was complete, the resultant cybrid cells were switched to cybrid growth medium, Optimem supplemented with 10% dialyzed FBS and 1% penicillin-streptomycin solution. Cybrid cell lines were grown in 75-cm^2 tissue culture flasks maintained in a humidified incubator at 37 °C and 5% CO_2. For Western blot analysis, caspase-1 determination and ELISA kits, cells were plated at a density of 2.5×10^6 cell/mL. For mitochondrial membrane potential and ROS production measurements using Amplex Red probe approximately 50000 cell/well were plated on 48-well plates. For live cell imaging and immunostaining approximately 25000 cells/well were plated on ibidi μ-Slide 8-well plates from GmbH (Germany) (Cat. No. 80821). The day after plating, cybrid growth medium as refreshed, and cells incubated with 1 μg/mL LPS 24 h, the higher concentration that did not reduce cell viability determined by the MTT-reduction test (SFig. 1b). Where indicated, 20 mM NH_4Cl and 100 mM leupeptin were added in the culture medium in the last 4 h of the treatment to monitor autophagy.

2.5. Rho0 and Rho + cells cell lines maintenance and treatments

Human pluripotent embryonal carcinoma (NT2) containing mitochondrial DNA (Rho+) and NT2 cells depleted of mtDNA (Rho0) were used. Rho+ and Rho0 cells were grown in 75 cm^2 tissue culture flasks in OPTIMEM medium containing 10% heat inactivated fetal calf serum, penicillin (50 U/ml), and streptomycin (50 μg/ml). The growth media for the Rho0 cells was further supplemented with uridine (50 μg/ml) and pyruvate (200 μg/ml). Cells were maintained at 37 °C in a humidified incubator containing 95% air and 5% CO2. For Western blot analysis, caspase-1 determination and ELISA kits, cells were plated in 6 well plates at a density of 2×10^6 cells/mL. For mitochondrial membrane potential and ROS production measurements using Amplex Red probe approximately 50000 cell/well were plated on 48-well plates. For live cell imaging and immunostaining approximately 25000 cells/well were plated on ibidi μ-Slide 8-well plates from GmbH (Germany) (Cat. No. 80821). After 24 h of plating, cells were treated with 1 μg/μL LPS for 24 h, the higher concentration that did not reduce cell viability determined by the MTT-reduction test (SFig. 1c). in medium without uridine and pyruvate. For all experimental procedures, controls were performed in the absence of LPS.

2.6. Mitochondrial function

2.6.1. Mitochondrial membrane potential analysis

Mitochondrial membrane potential (Δψm) was detected using the fluorescent dye TMRM. TMRM is a cell-permeant dye that accumulates in active mitochondria with intact membrane potentials. After treatment with LPS, mesencephalic neurons, cybrid cell lines and Rho+ and Rho0 cells were loaded with 300 nM of TMRM in HBSS (in the dark, at 37 °C) for 1 h. The fluorescence of TMRM (λexc = 540 nm; λem = 590 nm) was recorded using a Spectramax Plus 384 spectrofluorometer (Molecular Devices) during 5 min before (base line) and 3 min after mitochondrial depolarization with CCCP. Maximal mitochondrial depolarization (Δψm collapse) was performed by adding 1 μM CCCP (proton ionophore), which was always preceded by oligomycin (2 μg/ml) to prevent ATP synthase reversal. The dye retention was determined by the difference between maximum fluorescence (after depolarization) and the basal value of fluorescence and expressed in relation to untreated neurons/untreated control cybrids and untreated Rho + cells, respectively.

2.6.2. Analysis of hydrogen peroxide in neuronal mitochondria with MitoPY 1

To measure hydrogen peroxide in neuronal mitochondria Mitochondria peroxy yellow 1 (MitoPY1) probe was used [19]. MitoPY1 (Sigma Chemical Co., St. Louis, MO, USA) is a small-molecule fluorescent probe that selectively tracks to the mitochondria of live biological specimens and responds to local fluxes of hydrogen peroxide. After treatments neurons were washed with PBS 1 × and subsequently loaded in the dark with 10 μM MitoPY1 in HBSS without Phenol Red for 1 h. Then, primary neurons were washed with PBS 1x and HBSS without the probe was added. Basal Fluorescence was recorded for 5 min at 37 °C (λex = 503 nm and λem = 540 nm). Afterward, 5 μM Rotenone (Complex I inhibitor) was added to each well in order to achieve maximal ROS production. Measurements were recorded for 30 min at 37 °C. H202 production was calculated by the difference between the total fluorescence (after Rotenone) and the basal fluorescence. Results are expressed as a percentage of the dye retained within the untreated neurons. Measurements were performed using a Spectramax Plus 384 spectrofluorometer (Molecular Devices, Sunnyvale, CA, USA).

2.6.3. Analysis of hydrogen peroxide in cybrid cell lines and Rho0/Rho + cells with AmplexRed

Hydrogen peroxide was measured using Amplex® Red reagent (10-acetyl-3,7-dihydroxyphenoxazine) (ThermoFisher Scientific Inc, Waltham, MA USA). The Amplex® Red reagent in combination with horseradish peroxidase (HRP), was used to detect H_2O_2 in cybrid and Rho+/Rho0 cell lines after the treatment with LPS. In the presence of peroxidase, the Amplex® Red reagent reacts with H_2O_2 in a 1:1 stoichiometry to produce the red-fluorescent oxidation product, resorufin. After 24 h treatment with LPS cybrids and Rho+/Rho0 cell lines, were washed with PBS (1 ×) and subsequently loaded in the dark with 10 μM of Amplex® Red reagent and 0.5 U/ml HRP in HBSS without Fenol Red, and immediately placed on the fluorimeter. Fluorescence was recorded for 30 min at 37 °C (λex = 550 nm and λem = 580 nm). H_20_2 production was calculated as the slope after 30 min and results are expressed as fold increase in relation to untreated control cybrid cell lines or untreated and Rho + cells. Measurements were performed using a Spectramax Plus 384 spectrofluorometer (Molecular Devices, Sunnyvale, CA, USA).

2.6.4. Oxygen consumption rates measurement by seahorse XF24 extracellular flux analyzer

Mesencephalic neurons OCR was evaluated by seeding approximately 0.6 × 10^6 cells/mL per well in the 24 well cell culture microplates provided by the manufacturer (Agilent, Santa Clara, CA, USA; Cat. No. 100777–004). After 48 h exposure to LPS and 1 h before placing culture microplates in the Seahorse Analyzer, cells were washed in unbuffered DMEM (Cat. No. 5030) without HEPES and sodium bicarbonate and the media were then changed to the actual assay medium, which consisted of unbuffered DMEM containing 25 mM glucose, 1.82 mM sodium pyruvate and 2 mM L-glutamine, at pH 7.4. The microculture plates were de-gassed by placing in a non-CO_2 incubator at 37 °C for 1 h before the assay. OCR respiration measurements were made using a 30 s mix, 30 s wait, and 3 min read cycling protocol. During the first 3 reading periods basal OCRs were determined. After the third reading, wells were injected with 1 μM of oligomycin and the resulting OCR relative to ATP production, was measured over 3 cycles. After this, one injection of 2 μM FCCP were performed and OCR was recorded over 3 cycles, determining the maximum respiration and spare respiratory capacity. Finally, antimycin A (2 μM) was injected which measured the non-mitochondrial respiration and the resultant OCR was recorded over 3 reading cycles. The first OCR after antimycin injection provides the non-mitochondrial value to which all the described measurements were corrected.

2.6.5. 10-N-Nonyl acridine orange (NAO) staining

10-N-Nonyl acridine orange (NAO) binds to cardiolipin in all mitochondria, regardless of their energetic state as it is independent of mitochondrial membrane potential. Cardiolipin distribution and fluorescence was measured using the NAO probe. After treatments, mesencephalic neurons, cybrid cell lines and Rho+/Rho0 cells were washed with HBSS without phenol red and then loaded in the dark with 100 nM Cardiolipin in DMEM and Ham's F12 (Gibco, ThermoFisher Scientific, Waltham, MA, USA; Cat. No. 42400–028) without phenol-red for 1 h for cells and in HBSS for neurons. After a gentle wash, cybrid and Rho+/Rho0 cells were kept in DMEM during image acquisition whereas neurons were imaged in HBSS. Images were obtained using a Plan-Apochromat/1.4NA 63x lens on a Spinning Disk Cell Observer microscope (Zeiss Microscopy).

The images of cells stained with NAO were extracted to grayscale, inverted to show NAO-specific fluorescence as black pixels and thresholded to optimally resolve NAO staining. Background fluorescence and specific NAO fluorescence were determined. The final value for fluorescence intensity resulted from the subtraction of background fluorescence from specific fluorescence and the result was further divided by the number of cells (nucleus) from each acquired image.

2.6.6. Live cell imaging of mitochondrial trafficking

Mesencephalic neurons were seeded and differentiated on ibidi Treat μ-Slide 8-well plates. Following treatment with LPS, neurons were washed twice with HBSS [5.36 mM KCl, 0.44 mM KH2PO4, 137 mM NaCl, 4.16 mM NaHCO3, 0.34 mM NaH2PO4.H2O, 5 mM glucose, 5.36 mM Hepes, 0.001% Fenol Red, (pH 7.2)], and mitochondria was labeled with 100 nM MitoTracker Green (Invitrogen, Carlsbad, CA, USA) for 30 min at 37 °C in the dark, as previously described by our group [20] After a gentle wash, cells were kept in HBSS and imaged for mitochondrial movements. Timelapse images were captured under a Plan-Apochromat/1.4NA 63x lens on an Axio Observer.Z1 confocal microscope (Zeiss Microscopy, Germany) with Zeiss LSM 710 software with a stage-based chamber (5% CO2, 37 °C). The inverted microscope was driven by LSM software and images were taken every 2 s for a total of 10 min under × 63 magnification (Zeiss Plan-ApoChromat 63 × , 1.4NA). For transport analysis, mitochondria were considered no mobile if it remained stationary for the entire recording period. Movement was counted only if the displacement was more than the length of the mitochondrion (about 2 μm). For each time-lapse movie, mitochondria were manually tracked and transport parameters were generated using the ImageJ software plug-in Multiple Kymograph, submitted by J. Rietdorf and A. Seitz (European Molecular Biology Laboratory, Heidelberg, Germany). Movement velocity data were determined from the kymographic images and were calculated based on the slope (v = dx/dt) obtained for each profile along the recording time. Each series of images was recorded for at least three randomly selected MitoTracker Green neurons per culture and three independent cultures per condition.

2.6.7. Immunostaining

Mesencephalic neurons, were grown on glass coverslips (16 mm diameter) in 12-well plates whereas Rho0/Rho + cells and cybrid cell lines were grown in ibidi® μ-Slide eight-well plates from GmbH (Germany) (Cat. No. 80821). After treatment, neurons and cells were washed twice with serum-free medium and fixed with 4% paraformaldehyde for 20 min at RT. The fixed cells were washed again with PBS, permeabilized with methanol for 20 min at −20 °C (for LC3B) or with 0.2% Triton X-100 for 2 min at RT, and incubated with 3% BSA, to prevent non-specific binding, for 30 min. Then, cells were incubated with primary antibodies: 1:400 rabbit monoclonal anti-LC3 XP® from Cell Signaling (Danvers, MA, USA); 1:200 anti-SDHA (COXII) from Abcam (Cambridge; UK); 1:100 polyclonal anti-Tom20 from Santa Cruz Biotechnology (Santa Cruz, CA, USA); 1:100 anti-Lamp1 clone H4A3 from the Developmental Studies Hybridoma Bank (University of Iowa, Iowa City, IA, USA). Cells were then incubated with the appropriate secondary antibody (1:250 Alexa Fluor 594 or 1:250 Alexa Fluor 488 from Molecular Probes (Eugene, OR, USA)). Subsequently, cells were incubated with Hoechst 15 μg/μL for 5 min at RT and protected from light. After a final wash, the coverslips were immobilized on a glass slide with Mowiol 4–88 preparation for mounting medium (Sigma Chemical Co (St. Louis, MO, USA). Negative controls omitting each primary antibody were performed in each case, and no staining was seen. Images were acquired on a Zeiss LSM 710 (40 × 1.4NA plan-apochromat oil immersion lens) and analyzed using ImageJ software. Co-localization between Tom20/Lamp1; LC3/SDHA was quantified in threshold images with the JACoP plug-in of the ImageJ software, as previously described by our group [21]. A freely available ImageJ macro tool was used to analyze mitochondrial network as described in Valente and co-workers (2017) [22]. This macro allows the semi-automated analysis of mitochondrial networks in cultured mammalian cells as we have previously described [12].

2.7. Immunoblot analyses

To prepare cytosolic samples for TLR3 and TLR4 Western blot analyses, mesencephalic neurons, PD and control cybrids and Rho+/Rho0 cells were washed in ice-cold PBS and lysed in lysis buffer (10 mM HEPES; 3 mM $MgCl_2$; 1 mM EGTA; 10 mM NaCl, pH 7.5, supplemented with 2 mM DTT, 0.1 mM PMSF and a 1:1000 dilution of a protease inhibitor cocktail) supplemented with 0.1% Triton X-100. Neurons and cells were scraped on ice, transferred to the respective tubes and incubated on ice for 40 min. Afterward, samples were centrifuged at 2300×*g* for 10 min at 4 °C and the resulting supernatant contains the cytosolic fraction used to detect the proteins described above. For preparation of nuclear extracts for the analysis of p65 NF-κB, the resulting pellets were suspended in lysis buffer (20 mM HEPES, 300 mM NaCl, 5 mM $MgCl_2$, 0.2 mM EGTA, 20% glycerol, pH 7.5) supplemented with 2 mM DTT, 0.1 mM PMSF and a 1:1000 dilution of a protease inhibitor cocktail and samples were incubated on ice for 15 min. Subsequently, samples were centrifuged at 12000×*g* for 20 min at 4 °C and the resulting supernatant contains the nuclear fraction. To prepare samples for p62, LC3 and a-syn protein levels determination, neurons and cells were scraped on ice in hypotonic lysis buffer (25 mM HEPES, pH 7.5, 2 mM $MgCl_2$, 1 mM EDTA and 1 mM EGTA supplemented with 2 mM DTT, 0.1 mM PMSF and a 1:1000 dilution of a protease inhibitor cocktail) was supplemented with 1% Triton X-100. After 3 cycles of freezing (liquid nitrogen) and thawing (37 °C water bath), samples were centrifuged at 12000×*g* for 10 min and at 4 °C. The total amount of all resulting cell lysates obtained were removed and stored at −80 °C. Protein content was determined using BCA Protein Assay protein assay (Pierce; Cat. No. 23227).

For the analysis of mitochondrial phosphorylated DRP1 (p-DRP1), neurons were washed with PBS, scraped and disrupted on ice by homogenization in a buffer containing 250 mM sucrose, 20 mM Hepes, 1 mM EDTA, 1 mM EGTA, and protease inhibitors (0.1 M PMSF, 0.2 M DTT, 1:1000 dilution of a protease inhibitor cocktail and phosphatase inhibitors (1 tablet per 10 mL of lysis buffer) from Sigma Chemical Co (St. Louis, MO, USA; Cat. No. 04906845001)). This suspension was centrifuged at 500×*g* for 12 min at 4 °C. The resulting supernatant was centrifuged at 9500×*g* for 20 min at 4 °C. Pellets resulting from this step contain a crude mitochondrial fraction. Mitochondrial pellets were resuspended in sucrose buffer and freeze (liquid nitrogen) -thawed (37 °C water bath) three times. The total amount of resulting mitochondrial fractions obtained were removed and stored at −80 °C. For the analysis of α-synuclein oligomeric content samples were suspended in 2 × sample buffer (40% glycerol, 2% SDS, 0.2 M Tris-HCl pH 6.8, 0.005% Coomassie Blue) were not boiled (non-denaturing) and loaded under non-reducing conditions (in the absence of DTT in the sample buffer). For the analysis of the remaining proteins, samples were suspended in 6 × sample buffer and boiled for 5min at 95 °C (4 × Tris.HCl/SDS, pH 6.8, 30% glycerol, 10% SDS, 0.6 M DTT, 0.012% bromophenol blue). Depending on the protein molecular weight of interest, samples containing 35 μg of protein were loaded onto 10/15% SDS-PAGE gels. After transfer to PVDF membranes (Millipore, Billerica, MA, USA), non-specific binding was blocked by gently agitating the membranes in 3% BSA and 0.1% Tween-20 in Tris-Buffered Solution (TBS - 20 mM Tris, 150 mM NaCl and 0.1% (w/v) Tween-20 ®, pH 7.6) for 1 h at room temperature. The blots were subsequently incubated with the respective primary antibodies overnight at 4 °C with gentle agitation: 1:1000 anti-LC3B (Cat. No. 3868) from Cell Signaling (Danvers, MA, USA); 1:1000 anti-p62 (Cat. No. P0067) from Sigma Chemical Co (St. Louis, MO, USA); 1:1000 anti-p-Drp1 Serine 616 (Cat. No. 3455); 1:1000 anti-p65 NF-κB (Cat. No. 8242); 1:500 α-synuclein (Cat. No. ABN2265) from Sigma Chemical Co (St. Louis, MO, USA); 1:1000 TLR3 (Cat. No. ab84911) from Abcam (Abcam, Cambridge, UK); 1:500 TLR4 (Cat. No. sc-293072) from Santa Cruz Biotechnology (Santa Cruz, CA, USA). Finally, 1:1000 α-tubulin (Cat. No. T6199) from Sigma Chemical Co (St. Louis, MO, USA); 1:5000 β-actin (Cat. No. A5441) from Sigma Chemical Co (St. Louis, MO, USA) and 1:1000 anti-TOM20 (Cat. No. sc-11415) from Santa Cruz Biotechnology (Santa Cruz, CA, USA); 1:1000 anti-TATA binding protein (Cat. No. MAB3658) from Merk Life Science SLU (Sigma St. Louis, MO, USA) and 1:1000 βIII Tubulin (Cat. No. 4466) from Cell Signaling (Danvers, MA, USA) were used for loading control. Membranes were washed with TBS containing 3% BSA and 0.1% Tween three times (each time for 5 min), and then incubated with the appropriate horseradish peroxidase-conjugated secondary antibody for 2 h at RT with gentle agitation. After three washes, specific bands of interest were detected by developing with an alkaline phosphatase enhanced chemical fluorescence reagent (ECF from Sigma St. Louis, MO, USA) (Cat. No. GERPN3685). Fluorescence signals were detected using a BioRad ChemiDoc Imager, and band densities were determined using ImageLab software. Where indicated, protein densities were corrected with the densities of loading control proteins, to account for possible differences in protein loading.

2.8. Evaluation of inflammation markers by ELISA

After treatment with LPS, mesencephalic neurons and Rho+/Rho0 cells were washed in ice-cold PBS and proteins extracted in lysis buffer I (10 mM HEPES; 3 mM $MgCl_2$; 1 mM EGTA; 10 mM NaCl, pH 7.5) supplemented with 2 mM DTT, 0.1 mM PMSF and a 1:1000 dilution of a protease inhibitor cocktail and 0.1% Triton X-100. After 40 min of incubation on ice, samples were centrifuged at 2300×*g*, 10 min at 4 °C.

IL-1β and NF-κB levels were evaluated in 25 μg of cellular or

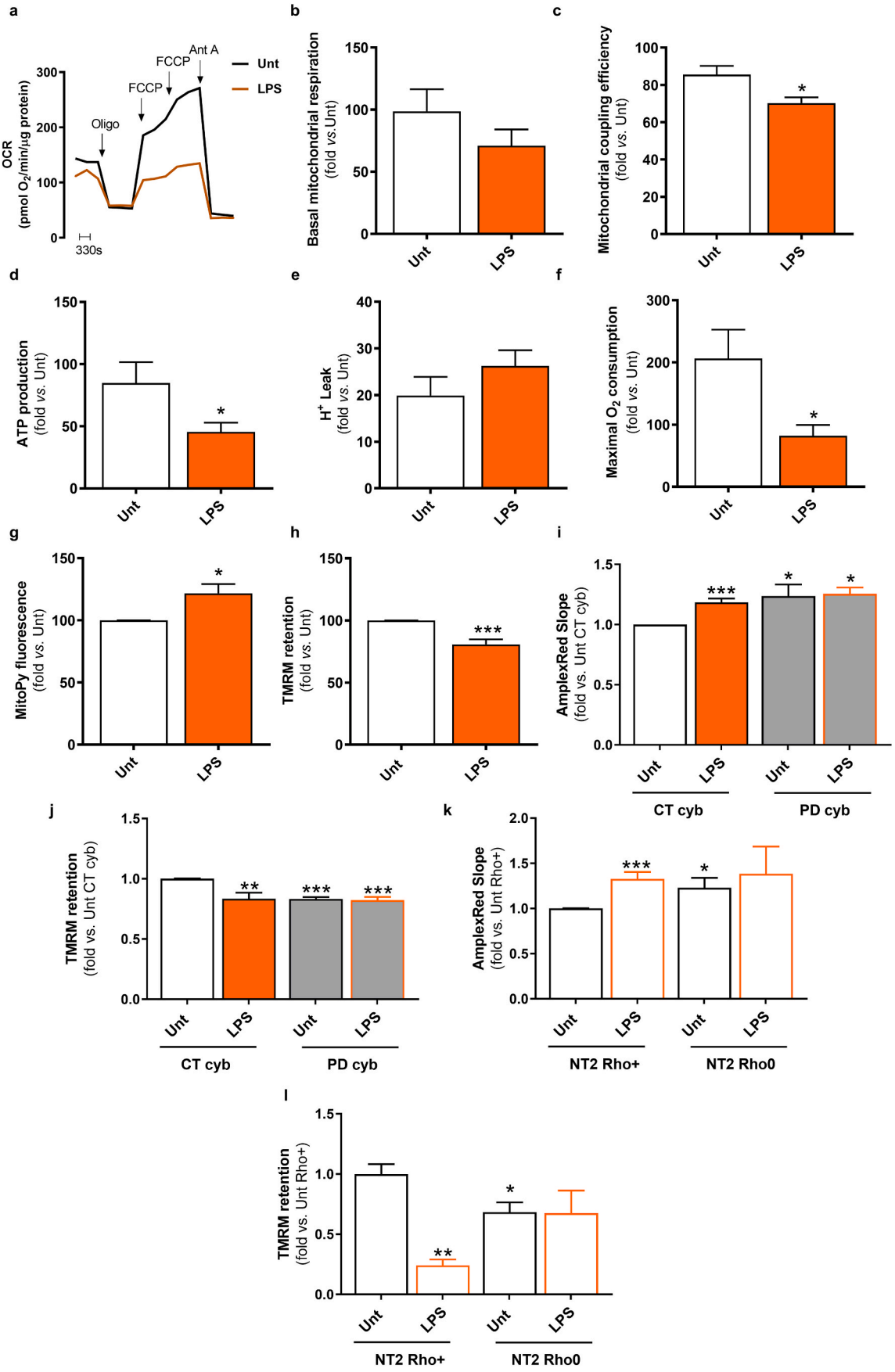

(caption on next page)

Fig. 1. Mitochondrial function is impaired upon LPS insult. LPS treated primary mice mesencephalic neurons. (a) Representative graph showing oxygen consumption rate (OCR); (b) basal respiration; (c) Mitochondrial coupling efficiency; (d) ATP production; (e) Proton leak; (f) Maximal oxygen consumption. (n = 4; *p < 0.05, relatively to untreated mesencephalic neurons). (g) Mitochondrial ROS production. (n = 5; *p < 0.05, relatively to untreated mesencephalic neurons) (h) Changes in mitochondrial membrane potential. (n = 6; ***p < 0.001, relatively to untreated mesencephalic neurons). CT and PD cybrids exposed to LPS. (i) ROS production. (n = 5; *p < 0.05 and ***p < 0.001, relatively to untreated CT cybrids). (j) Changes in mitochondrial membrane potential. (n = 5; **p < 0.01 and ***p < 0.001, relatively to untreated CT cybrids). NT2-Rho+ and -Rho0 cells treated with LPS. (k) ROS production. (n = 5–8; *p < 0.05 and ***p < 0.001, relatively to untreated NT2 Rho+). (l) Changes in mitochondrial membrane potential. (n = 3–6; *p < 0.05 and **p < 0.01, relatively to untreated NT2 Rho+).

neuronal extracts using Quantikine ELISA (R&D Systems; Cat. No. MLB00C) and NFκB p65 Total SimpleStep ELISA Kit (Abcam; Cat. No. ab176648), respectively, according to manufacturer's instructions. Absorbance was registered at 450 nm in a SpectraMax Plus 384 multiplate reader. Results were expressed as μg/ml protein for NFκB p65 and as pg/mL for IL-1β.

2.9. Assessment of a-syn oligomers levels

The concentration of a-syn oligomers was determined in 25 μg of neuronal extracts with the a-syn oligomer (SNCO α) ELISA Kit (MyBioSource; Cat. No. MBS724099). Absorbance was read at 450 nm in a SpectraMax Plus 384 multiplate reader. Results were expressed as pg/mL.

2.10. Caspase 1-like activity assay

Mesencephalic neurons, cybrid and Rho+/Rho0 cell extracts were processed as described above for ELISA kits. The resultant cell extracts were removed and stored at −80 °C. Protein content was determined using BCA Protein Assay protein assay (Pierce).

Caspase 1 activation was measured using a colorimetric substrate, VAD (Val-Ala-Asp), in which the substrate cleavage was monitored at 405 nm. Lysates containing 40 μg protein were incubated at 37 °C for 2 h in 25 mM HEPES, pH 7.5 containing 0.1% CHAPS, 10% sucrose, 2 mM DTT and 40 μM of Ac-VAD-4-methoxy-2-naphtylamide (Sigma St. Louis, MO, USA) to determine caspase 1 activation. Detection was evaluated at 405 nm using a Spectramax Plus 384 spectrophotometer (Molecular Devices, Sunnyvale, CA, USA).

2.11. Data analysis

Data are expressed as means ± standard error of the means (SEM) of at least 4 independent experiments. Statistical analyses were performed using GraphPad Prism 6 for Windows (GraphPad Software, San Diego, CA, USA). To compare means between groups we used one-way analysis of variance (ANOVA) followed by Dunnett's multiple comparisons (comparisons between untreated neurons/cells *versus* treatments) or Student's *t*-test. p-values <0.05 were considered significant.

3. Results

3.1. LPS induces mitochondrial morphofunction impairment in mesencephalic neurons but not in PD cybrids and Rho0 cells

Previous data have shown that LPS causes mitochondrial failure [12] resulting in ultrastructural changes and subsequent dopaminergic neuronal death [23] both in vitro and *in vivo*. Herein we exposed mesencephalic neurons, CT and sPD cybrid cells and mtDNA-depleted cells to LPS in concentrations that did not interfere with cell viability (data not shown). We demonstrate that exposing mesencephalic neurons to 1 μg/μL of LPS during 48 h, results in reductions in mitochondrial OCR, with significant decreases in mitochondrial coupling efficiency, ATP production and maximal O_2 consumption (Fig. 1a–f). These differences in mitochondrial OCR were accompanied by an increase in mitochondrial ROS production and a decrease in mitochondrial membrane potential (Fig. 1g–h). Similarly, we observed that CT cybrids and NT2 Rho + cells exposed to LPS also show an increase in mitochondrial ROS production and a decrease in mitochondrial membrane potential (Fig. 1i-l). Interestingly, in hybrid cells harboring sPD patient mitochondria already show at baseline an increase in ROS production and a decrease in mitochondrial membrane potential (Fig. 1i–j) and LPS was unable to further aggravate these deficits. NT2 Rho0 cells do not have a functional electron transport chain but with pyruvate and uridine supplementation are able to maintain ATP levels and mitochondrial membrane potential through glycolysis [24,25]. Our results with pyruvate and uridine depleted medium show an increase in ROS production and a decrease in mitochondrial membrane potential in untreated NT2 Rho0 cells (Fig. 1k-l) [24].

Mitochondrial membrane potential collapse is correlated with alteration in mitochondrial dynamics and morphology [25]. In LPS-treated primary mesencephalic neurons we observed an increase in mitochondrial phospho-Drp1 (Fig. 2a–b). Drp1 primarily resides in the cytosol, but can be recruited to mitochondria and promote mitochondrial fission [26]. To evaluate mitochondrial distribution and morphology, we used TOM20 staining and determined the number of mitochondria individuals and network size using a Macro from ImageJ. We observed that in accordance with the increase in phospho-Drp1 mitochondrial levels, the number of mitochondria individuals is increased whereas the mitochondria network size is reduced indicating mitochondrial fragmentation (Fig. 2c–e). Similarly, CT cybrids (Fig. 2 f-h) and NT2 Rho + cells (Fig. 2i–k) exposed to LPS show a decrease in the number of mitochondria network size. Interestingly, we found that both untreated PD cybrids and NT2 Rho0 show fragmented mitochondria as observed by an increase in the number of fissed mitochondria (mitochondrial individuals) (Fig. 2g and j). On the other hand, in PD cybrids LPS did not affect the number of mitochondrial individuals but decreased the mitochondria networks size (Fig. 2g–h). Similarly, in NT2 Rho0 cells no statistically significant effect was observed following LPS exposure (Fig. 2j–k).

Subsequently, we evaluated cardiolipin exposure since this phospholipid is abundant in the inner mitochondrial membrane and is implicated in mitochondrial dynamics and respiratory chain enzyme activity [27]. Treatment of primary mesencephalic neurons with LPS triggered cardiolipin exposure (Fig. 3a–b). Remarkably, PD cybrids already show an increase in cardiolipin fluorescence intensity indicating its exposure (Fig. 3c–d). Additionally, cardiolipin exposure was reduced in NT2 Rho0 cells (Fig. 3e–f), which indicates that the biosynthesis of cardiolipin in these cells may be altered. LPS failed to increase cardiolipin exposure in PD cybrids and Rho0 cells.

The preservation of a healthy mitochondrial network heavily depends on mitochondrial dynamics and mitophagy, hence the accumulation of dysfunctional and fragmented mitochondria is expected to be removed by mitophagy. Therefore, we evaluated mitochondrial movement and macroautophagy in mesencephalic neurons. We first detected that LPS led to a reduction in mitochondrial average velocity (Fig. 4a–b) which was correlated with an increase in the accumulation of autophagosomes and a decrease in autophagic flux (Fig. 4c–e) indicating that macroautophagy was impaired. Similarly, we found that hybrid cells harboring sPD patient mitochondria and mtDNA-depleted cells have an inherent reduced autophagic flux when compared to CT cybrids and NT2 Rho + cells, respectively (Fig. 4l-q). In addition, LPS does not further

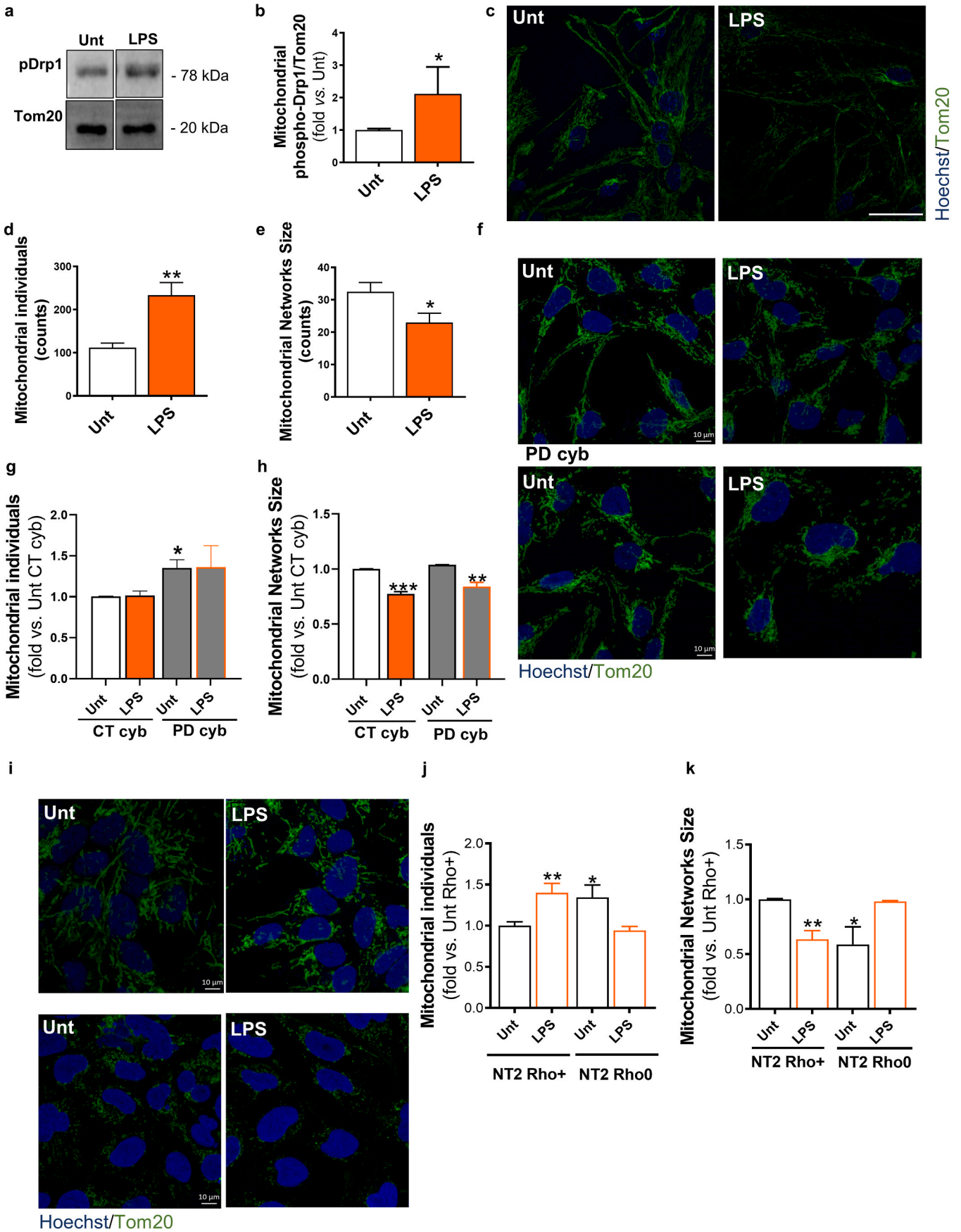

(caption on next page)

Fig. 2. LPS-induced mitochondria dynamics and network disruption. LPS treated primary mice mesencephalic neurons. (a) Representative immunoblot for phospho-Drp1. (b) Densitometric analysis of phospho-Drp1. (n = 4; *p < 0.05, relatively to untreated mesencephalic neurons). (c) Representative images of mitochondrial network immunostained with Tom20. Scale bar: 50 μm. (d) Number of mitochondrial individuals. (e) Number of mitochondrial network size. (n = 4; *p < 0.05 and **p < 0.01, relatively to untreated mesencephalic neurons). CT and PD cybrids exposed to LPS. (f) Representative images of mitochondrial network immunostained with TOM20. Scale bar: 10 μm. (g) Number of mitochondrial individuals. (h) Number of mitochondrial network size. (n = 3; *p < 0.05, **p < 0.01 and ***p < 0.001, relatively to untreated CT cybrids). NT2 Rho+ and Rho0 cells treated LPS. (i) Representative images of mitochondrial network immunostained with TOM20. Scale bar: 10 μm. (j) Number of mitochondrial individuals. (k) Number of mitochondrial network size. (n = 4–7; *p < 0.05 and **p < 0.01, relatively to untreated NT2 Rho+).
Hoechst 33342-stained nuclei are in blue. (For interpretation of the references to color in this figure legend, the reader is referred to the Web version of this article.)

exacerbate autophagic flux failure. We also found that in mesencephalic neurons exposed to LPS mitochondria were less co-localized with autophagosomes (Fig. 4f–h) and saw a tendential decrease in mitochondria co-localization with autolysosomes (Fig. 4i–k). These results suggest a deficient signalling in the engulfment of mitochondria by the autophagosomes potentially leading to a decreased turnover of dysfunctional mitochondria.

3.2. Inherent or LPS-induced mitochondrial dysfunction activates innate immunity components

Cardiolipin, ROS, mtDNA and ATP are known DAMPs that upon mitochondrial fragmentation can be exposed and can modulate inflammasome localization and activation [28]. Since we previously observed that LPS induced mitochondrial dysfunction concomitant with

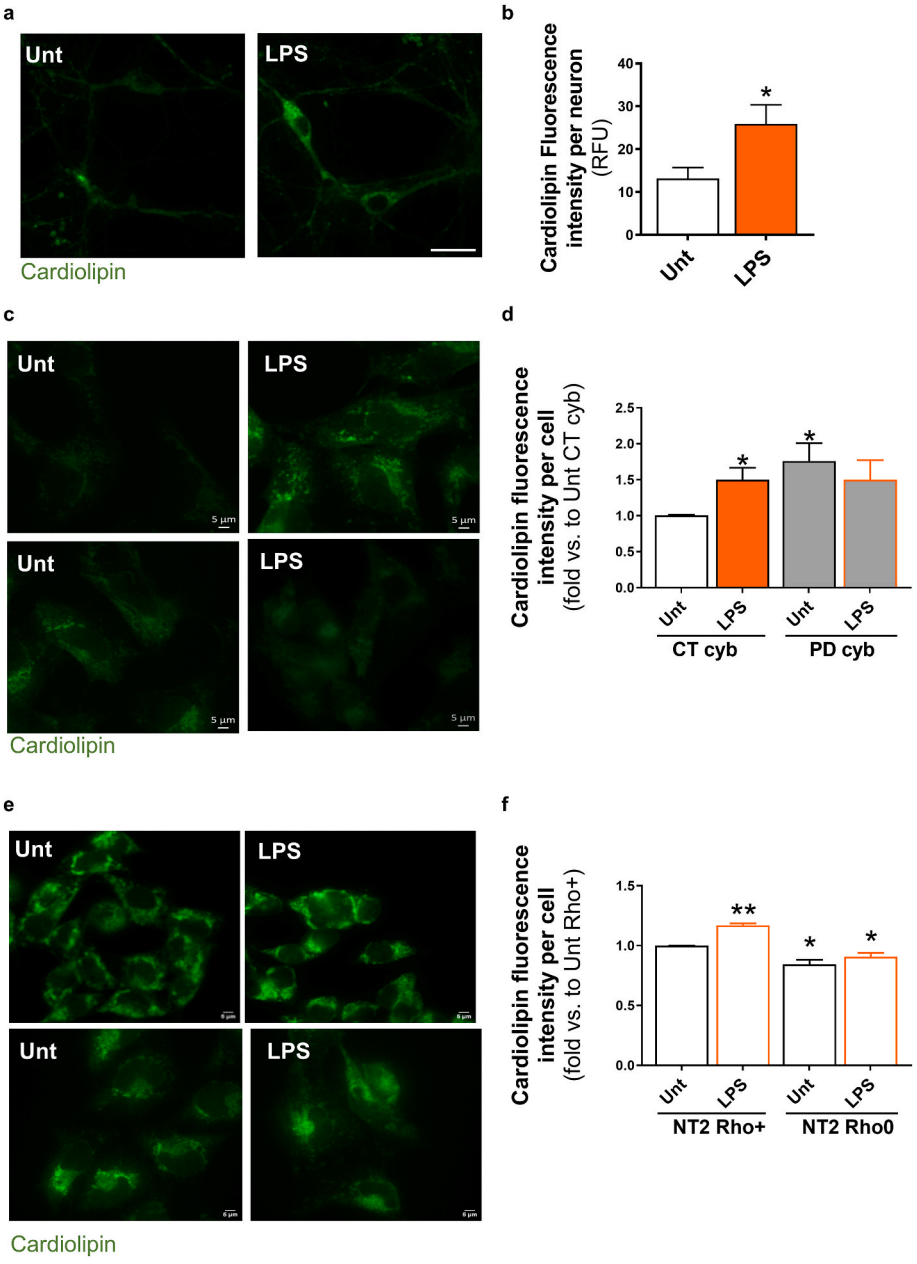

Fig. 3. LPS promotes cardiolipin exposure through mitochondria network disturbance. Primary mice mesencephalic neurons treated with LPS. (a) Representative image of cardiolipin exposure. Scale bar: 30 mm. (b) Cardiolipin fluorescence intensity. (n = 6; *p < 0.05, relatively to untreated mesencephalic neurons). CT and PD cybrids exposed to LPS. (c) Representative image of cardiolipin exposure. Scale bar: 5 μm. (d) Cardiolipin fluorescence intensity. (n = 3; *p < 0.05, relatively to untreated CT cybrids). NT2-Rho+ and -Rho0 cells treated with LPS. (e) Representative image of cardiolipin exposure. Scale bar: 5 μm. (f) Cardiolipin fluorescence intensity. (n = 3; *p < 0.05 and **p < 0.01, relatively to untreated NT2 Rho+).

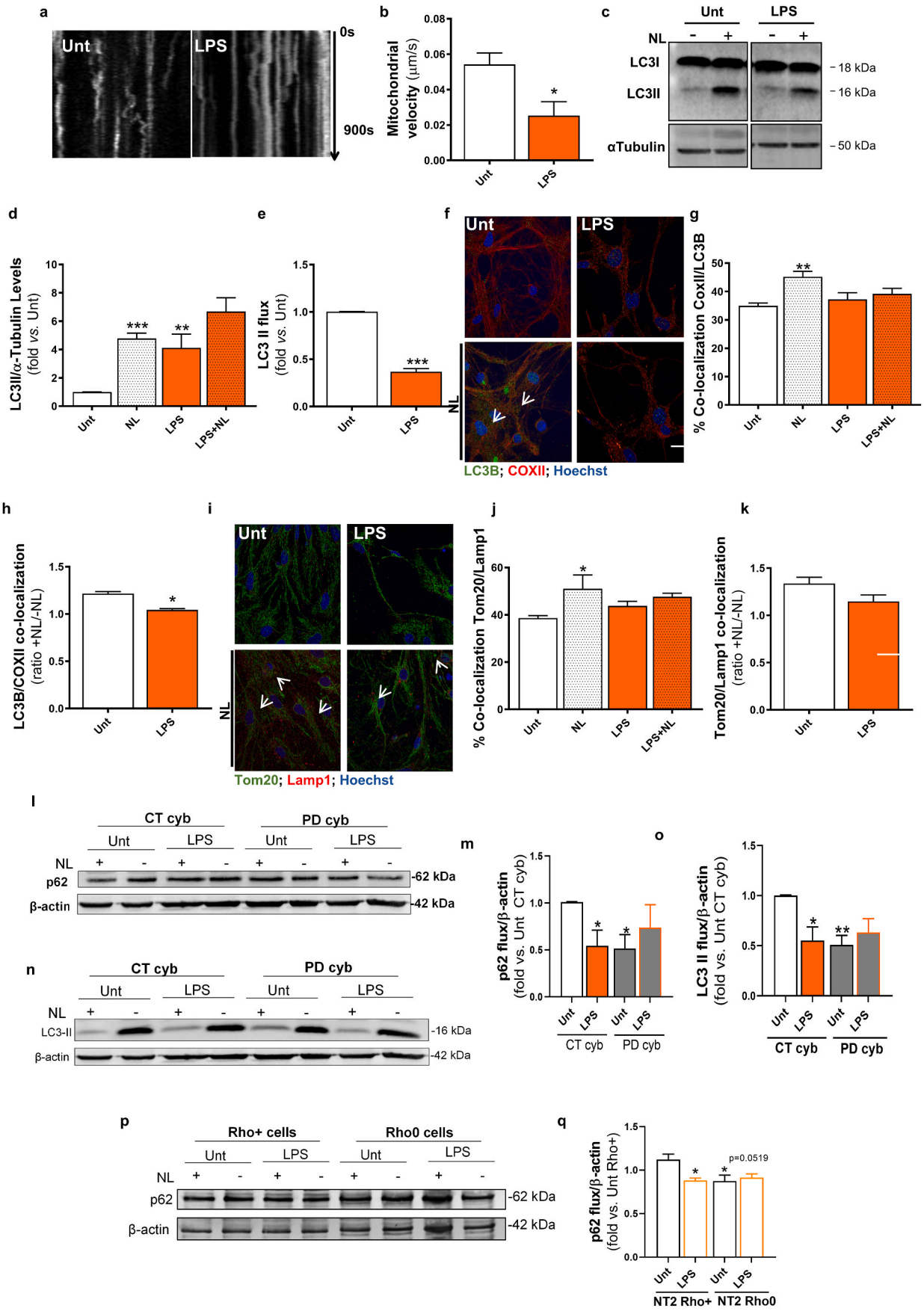

(caption on next page)

Fig. 4. Autophagic response impairment in cells that lack functional mitochondria and in LPS-exposed mesencephalic neurons. Primary mice mesencephalic neurons treated LPS. (a) Representative kymograph images of mitochondrial movement. Scale bars: 5 μm. (b) Average transport velocity of mitochondria. (n = 6; *p < 0.05, relatively to untreated mesencephalic neurons). (c) Representative immunoblot for endogenous LC3B. (d) Determination of autophagosomes levels (LC3-II basal densitometric values). (e) Assessment of autophagic flux, determined as the ratio of LC3-II densitometric value of NL-treated samples over the corresponding untreated samples. (n = 4; **p < 0.01 and ***p < 0.001, relatively to untreated mesencephalic neurons). (f) Co-localization between autophagic vacuoles and mitochondria. (g–h) Assessment of LC3B and SDHA co-localization (n = 4; *p < 0.05 and **p < 0.01, relatively to untreated mesencephalic neurons). (i) Co-localization between mitochondria and lysosomes. (j–k) Assessment of Tom20 and Lamp1 co-localization. (n = 4; *p < 0.05, relatively to untreated mesencephalic neurons). Scale bars: 30 μm. CT and PD cybrids exposed to LPS. (l) Representative immunoblot for p62. (m) Assessment of autophagic flux, determined as the ratio of p62 densitometric value of NL-treated samples over the corresponding untreated samples. (n = 4; *p < 0.05, relatively to untreated CT cybrids). (n) Representative immunoblot for endogenous LC3B. (o) Assessment of autophagic flux. (n = 4; *p < 0.05 and **p < 0.01, relatively to untreated CT cybrids). NT2 Rho+ and NT2 Rho0 cells treated with LPS. (p) Representative immunoblot for p62. (q) Assessment of autophagic flux. (n = 3; *p < 0.05, relatively to untreated NT2 Rho+). Hoechst 33342-stained nuclei are in blue. (For interpretation of the references to color in this figure legend, the reader is referred to the Web version of this article.)

an increase in cardiolipin exposure in primary mesencephalic neurons, we decided to evaluate NLRP3 inflammasome, an innate immune sentinel involved in neuronal innate immunity. Additionally, Toll-like Receptor-4 (TLR4) mediates LPS-induced signal transduction [29]. In neurons we found that TLR4 levels were increased after LPS treatment (Fig. 5a–b). TLR4 is an important Pattern Recognition Receptor (PRR) placed in the plasma membrane that plays an important role in initiating the innate immune response [29]. This receptor can signal NF-κB, which will activate NLRP3 inflammasome. Accordingly, we detected an increase in NF-κB levels (Fig. 5c). Moreover, we observed Caspase-1 activation (Fig. 5d) and an increase in pro-inflammatory IL-1β production (Fig. 5e). Remarkably, in cells harboring PD patient mitochondria LPS did not augment the pro-inflammatory response as it was already in motion. PD cybrids already show at baseline an increase in TLR3 levels (Fig. 5f–g). TLR3 is also an PRR that localizes both at the cell surface and in endosomes and its signalling pathway also activates transcription factors, namely NF-κB thus mediating the production of pro-inflammatory cytokines [30]. Indeed, we observed an increase in nuclear NF-κB p65 protein levels (Fig. 5h–i), and an increase in caspase-1 activation (Fig. 5j) and pro-inflammatory IL-1β levels (Fig. 5k) in untreated PD cybrids. However, we did not detect the same response in untreated NT2 Rho0 cells. Comparatively with NT2 Rho + cells we observed an activation of caspase-1 and increased IL-1β levels (Fig. 5p-q). LPS triggered a pro-inflammatory response in CT cybrids and NT2 Rho + cells, but failed to do so in PD cybrids and Rho0 cells. Taken together, our results strongly suggest that mitochondrial dysfunction either inherent or induced by LPS activates a pro-inflammatory response which is an important component of the innate immunity response probably as a result of the exposure of mitochondrial DAMPs.

3.3. *a-Syn oligomerization is a response of innate immunity process*

a-Syn is the major component of intraneuronal protein aggregates, the so-called LBs, the major histopathological hallmark of PD. However, studies have also suggested that aggregates formation is a protective mechanism whereas oligomers and pre-fibrillar a-syn are the toxic species responsible for neurodegeneration [31]. Although it remains unknown how LPS-derived neuroinflammation contributes to the loss of dopaminergic neurons in PD, several mechanisms have been described to play a role in DA neuronal death. Moreover, a growing body of evidence suggests that a-syn shares antimicrobial-like properties [10]. We then sought to evaluate whether the activation of innate immunity responses either induced by inherent mitochondrial dysfunction or induced by LPS could lead to the accumulation of a-syn oligomers. Our results show that mesencephalic neurons challenged with LPS for 48 h have an increase in cytosolic (Fig. 6a) and mitochondrial (Fig. 6b–c) a-syn oligomers. Additionally, untreated PD cybrids (Fig. 6b–c) and NT2 Rho0 cells (Fig. 6d–e) already exhibit the accumulation of a-syn oligomers, comparing with age-matched control cybrids and NT2 Rho + cells, respectively. Moreover, we found that LPS exposure is unable to aggravate a-syn production in cells with mitochondrial deficits. Regarding, NT2 Rho + cells and CT cybrids we found that LPS triggers a-syn oligomers accumulation indicating that a bacterial toxin can trigger a-syn pathology.

4. Discussion

Mitochondria dysfunction and (neuro)inflammation are two prominent pathological features involved in neurodegenerative diseases, including PD. Herein, we present evidence that cells harbouring PD patient mitochondria with inherent mitochondrial deficits trigger and activate, without any insult, sentinel components of innate immunity response. Most interestingly, in mtDNA-depleted cells with no functional mitochondria LPS was not able to induce a pro-inflammatory response. Furthermore, we demonstrate that this bacterial toxin induces mitochondrial dysfunction while causing inflammation in enriched primary mesencephalic neurons with little contribution from the microglia. Indeed, accumulating evidence posits mitochondria multifaceted role in inflammatory responses. Mitochondria can act as a signalling platform for the activation of the NLRP3 inflammasome playing an important role in inflammatory responses. Importantly, the inflammasome can be activated by pathogen associated molecular patterns (PAMPS), such as LPS, proteoglycans and double stranded RNA but also by endogenous signals, DAMPs, which can include mtDNA, cardiolipin, ROS and ATP [32]. It is very well documented that among PAMPs, LPS has a prominent role in mitochondria function leading to enhanced mitochondrial fission and fragmentation, increased ROS production, deficient mitophagy and microglial inflammation. This was shown in microglial cells [33,34], macrophages [35,36] and *in vivo* [37,38]. Our work is the first to show that in enriched mesencephalic neuronal cultures with low levels of glial cells (less than 1% of Iba1-, Trem2-, CD11b-positive cells and less than 20% of GFAP-positive cells). LPS activates neuronal innate immunity, namely NF-κB and other transcription factors that may also signal aSyn expression. Accumulating evidence supports the notion that non-immune cells are capable of inducing innate immune responses, including neurons [39]. Indeed, neurons can express TLR3 and TLR4 [12,13] and produce inflammatory cytokines, such as IL-6 and TNF-α mediating innate immunity in the absence of microglial cells [40]. Moreover, our group reported that, similarly to LPS, a bacterial neurotoxin, namely BMAA activated the NLRP3 inflammasome accompanied by the release of IL-1β in both pure cortical and enriched mesencephalic neuronal cultures [12,13]. Herein, our data reveal that LPS activates innate immunity responses by inducing mitochondrial impairment which results in increased mitochondrial fragmentation with concomitant cardiolipin exposure in pure mesencephalic neurons. Most interestingly, in this study we demonstrate that in cells with dysfunctional mitochondria (PD cybrids) with a fragmented mitochondrial network, cardiolipin is inherently exposed to the outer mitochondrial membrane. Cardiolipin is in fact a hallmark lipid of mitochondria also found in the membrane of bacteria and is critically involved in a multitude of mitochondrial and cellular processes [41]. However, upon a pathogenic insult cardiolipin is translocated from the

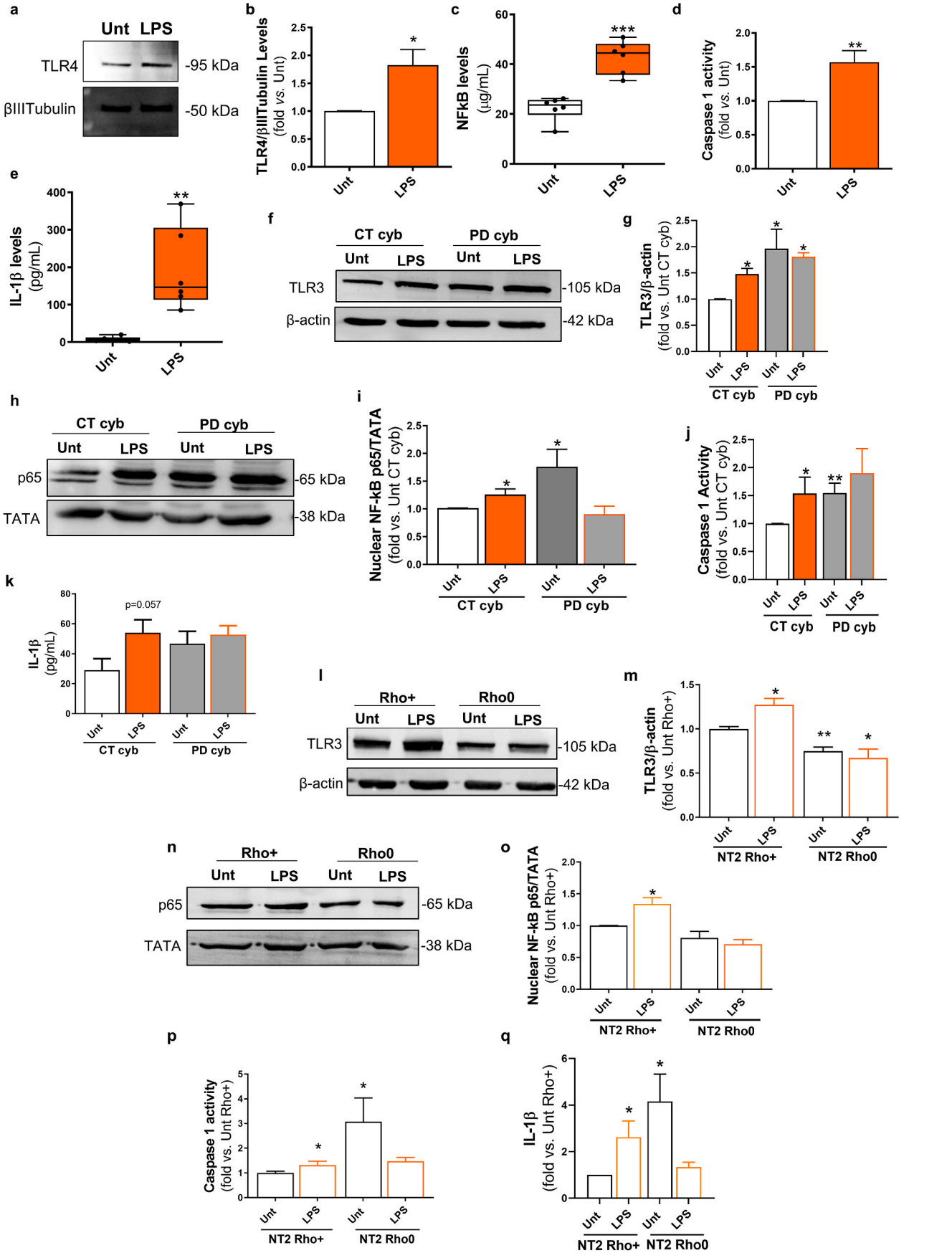

(caption on next page)

Fig. 5. LPS-induced mitochondrial dysfunction activates innate immunity. Primary mice mesencephalic neurons treated with LPS. (a) Representative immunoblot for TLR4 levels. (b) Densitometric analysis of TLR4. (n = 5; *p < 0.05, relatively to untreated mesencephalic neurons). (c) NF-κB levels. Values are in μg/mg protein. (n = 6; ***p < 0.001, relatively to untreated mesencephalic neurons). (d) Caspase-1 activation. (n = 6; **p < 0.01, relatively to untreated mesencephalic neurons). (e) Cytosolic IL-1β levels. (n = 6; **p < 0.01, relatively to untreated mesencephalic neurons). CT and PD cybrids exposed to LPS. (f) Representative immunoblot for TLR3 levels. (g) Densitometric analysis of TLR3. (n = 4; *p < 0.05, relatively to untreated CT cybrids). (h) Representative immunoblot of nuclear p65 NFκB. (i) Densitometric analysis of nuclear p65 NFκB. (n = 5; *p < 0.05, relatively to untreated CT cybrids). (j) Caspase-1 activation. (n = 6; *p < 0.05 and **p < 0.01, relatively to untreated CT cybrids). (k) Cytosolic IL-1β levels. (n = 6; CT cybrid Unt vs CT cybrid LPS, p = 0.057). NT2 Rho+ and Rho0 cells were treated with LPS. (l) Representative immunoblot for TLR3 levels. (m) Densitometric analysis of TLR3. (n = 4; *p < 0.05 and **p < 0.01, relatively to untreated NT2-Rho+). (n) Representative immunoblot of nuclear p65 NFκB. (o) Densitometric analysis of nuclear p65 NFκB. (n = 3; *p < 0.05, relatively to untreated NT2 Rho+). (p) Caspase-1 activation. (n = 6; *p < 0.05, relatively to untreated NT2-Rho+). (q) Cytosolic IL-1β levels. (n = 4; *p < 0.05, relatively to untreated NT2-Rho+).

inner to the outer mitochondrial membrane playing a critical role in the activation of the NLRP3 inflammasome. Activation of the NLRP3 inflammasome involves both priming and activation steps [42]. In the priming step, inflammatory LPS triggers TLR4 and induces the NF-κB-mediated expression of NLRP3, pro-IL-1β and pro-caspase-1. After priming, NLRP3 responds to activating stimuli (such as DAMPs) and assembles the NLRP3 inflammasome complex. In this study, we found that mesencephalic neurons exposed to LPS show an increase in TLR4 expression signalling NF-κB translocation into the nucleus, which upon activation by cardiolipin exposure induced the release of pro-inflammatory cytokines, namely IL-1β. Similarly, in untreated PD cybrids TLR3 expression and NF-κB translocation into the nucleus is increased contributing to caspase-1 activation and IL-1β release. Interestingly, Rho0 cells show increased inflammation but LPS was not capable of initiate a pro-inflammatory response. Indeed, in PD cybrids the increase in cardiolipin levels could be responsible for NLRP3 direct activation as it was previously described that cardiolipin can bind to NLRP3 directly to induce its activation [43]. In Rho0 cells without mtDNA and decreased levels of cardiolipin we hypothesize that mitochondrial ROS overproduction induces NLRP3 activation via thioredoxin/thioredoxin-interacting protein [44]. Our results further reinforce and highlight the importance of mitochondria in innate immune pathways. Interestingly, in mice intraperitoneally injected with LPS, neuronal mitofusin-2 overexpression abrogated LPS-induced pro-inflammatory responses [37]. In addition, Park and colleagues reported that in primary microglia cells LPS induced a pro-inflammatory response which was mediated by mitochondrial ROS [34]. Exposed cardiolipin has also been shown to mediate the degradation of damaged intracellular mitochondria and phagocytosis of mitochondria from the extracellular milieu [41]. However, we observed a decreased turnover of dysfunctional mitochondria in LPS-exposed neurons. It is well established that intracellular trafficking and autophagic turnover maintenance are highly dependent on mitochondrial function [45]. Interestingly, our data suggests that LPS by impairing mitochondrial function leads to the disruption of microtubule-dependent trafficking which ultimately affects macroautophagy. This is confirmed in both NT2 Rho + cells and CT cybrids where LPS reduces the autophagic flux. Corroborating this data, it has been shown that LPS suppressed the autophagic flux in microglial cells and mice [46–48] by inhibiting autophagosome formation. On the other hand, LPS has also been shown to induce autophagy in cardiomyocytes [49] and osteoclasts [49] as a cytoprotective response to LPS-induced injury. Autophagy is indeed a double-edged sword playing a role in cell survival as well as in cell death [50,51]. These studies indicate that in some settings LPS-induced autophagy inhibition can participate in the excessive pro-inflammatory response whereas in others can promote autophagy as a protective response.

a-Syn accumulation is a hallmark of PD neuropathology and is a known autophagic substrate [52]. We found that LPS triggered a-syn accumulation in the cytosol and mitochondria of mesencephalic neurons. Moreover, since PD cybrids already show high levels of a-syn LPS did not exacerbated its accumulation. This was also observed in cells without functional mitochondria (NT2 Rho0). Several reports from our group have consistently reported that hybrid cells harboring PD patient mitochondria recapitulate several pathogenic features observed in PD subject brains including the accumulation of dysfunctional mitochondria and a-syn oligomers [45,53]. Importantly, in both PD cybrids and NT2 Rho0 cells LPS did not contributed to a further increase in a-syn oligomerization. Recently, several reports suggested that a-syn can act as an antimicrobial peptide since it shares many biophysical characteristics. In fact, Park and co-workers demonstrated that a-syn harbours antibacterial activity against *Escherichia coli* and *Staphylococcus aureus* [10]. Another report shows that colonization of mice overexpressing the human amyloid a-syn with curli-producing gut bacteria accelerates a-syn pathology in the gut and the brain and exacerbates motor dysfunction [54]. Our results corroborate these data since we show that a bacterial toxin can promote a-syn aggregation through activation of innate immunity. On the other hand, a-syn can also induce pro-inflammatory responses since the injection of a-syn fibrils into the SNpc induce the recruitment of peripheral immune cells to the central nervous system [55]. Additionally, a-syn oligomers showed high affinity for TLR4 and induced an inflammatory response in glial cells characterized by increased TNF-α and IL-1β production [56]. It was demonstrated that aSyn overexpression induces mitochondrial dysfunction [57]. We have previously demonstrated that aSyn accumulates in the mitochondria after incubation of neurons with a bacterial neurotoxin [13] and with an *alpha-proteobacteria* [58]. In this report, we propose that LPS stimulates a-syn oligomerization trough innate immunity and enters the mitochondria promoting the collapse of mitochondrial membrane potential, its fragmentation and ROS production. In cells that already contain dysfunctional mitochondria, like PD cybrids, LPS even after the activation of TLRs or NLRs do not have an additive effect. For Rho0 cells without a functional mitochondria we observe the same effect. Hunter and colleagues demonstrated that intrastriatal injection of LPS in rats induced an inflammatory response where mitochondrial deficits were correlated with the loss of dopaminergic neurons in the SNpc [23]. Moreover, stereotaxic injection of LPS into the SNpc induced an inflammatory reaction and selective degeneration of nigrostriatal dopaminergic neurons [59].

Our results provide evidence for the first time that without a functional mitochondria LPS is not able to activate an inflammatory response. Our findings further highlight the crucial role of mitochondrial dysfunction in PD pathogenesis working as a signalling hub platform for a-syn pathology induced by neuronal innate immune activation.

Funding

This work was supported by the European Regional Development Fund (ERDF), through the COMPETE 2020 – Operational Programme for Competitiveness and Internationalization and by Portuguese national funds via FCT—Fundação para a Ciência e a Tecnologia under projects PTDC/MED-NEU/3644/2020, UIDB/04539/2020, UIDP/04539/2020 and LA/P/0058/2020.

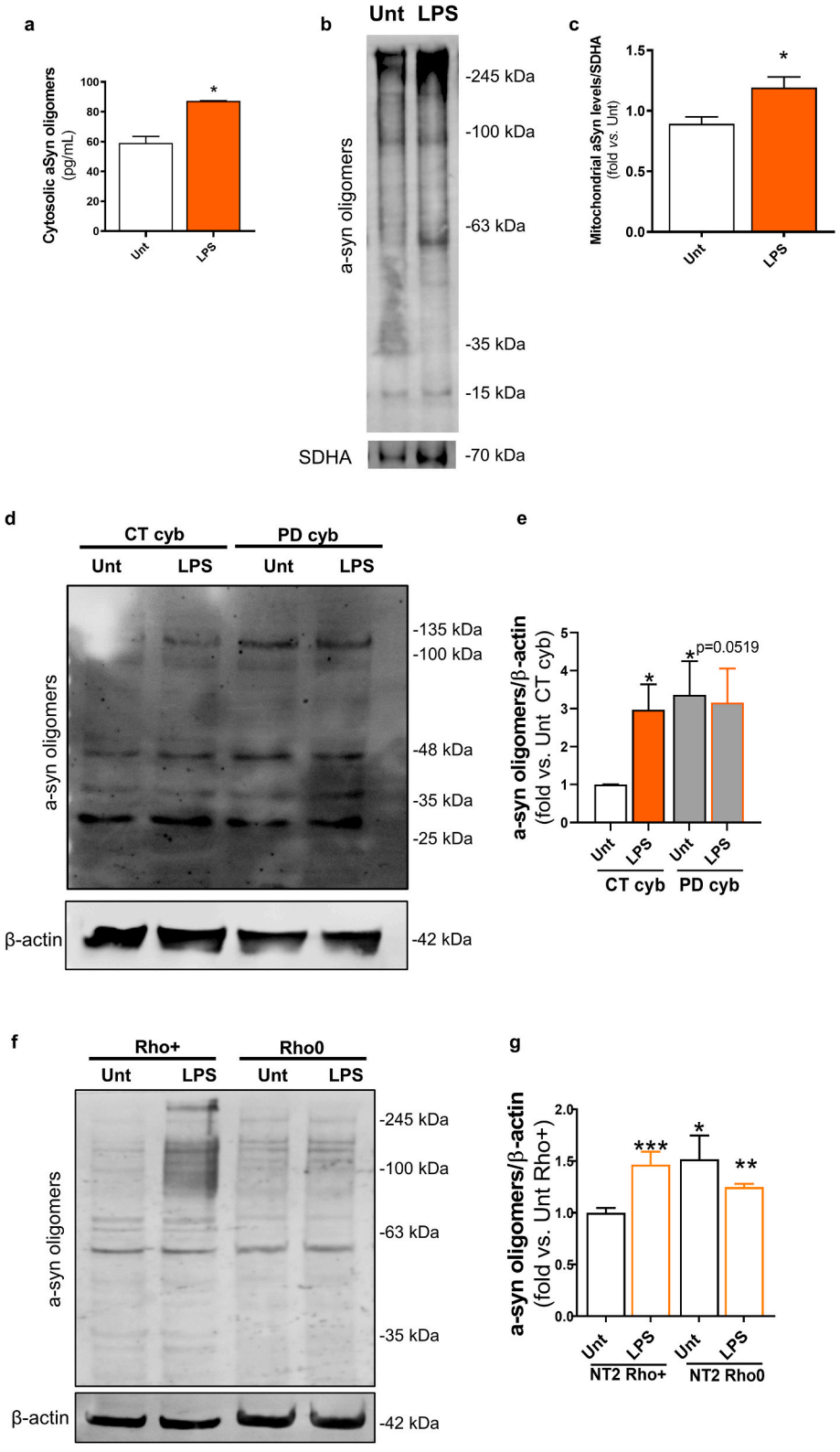

Fig. 6. LPS insult culminates in a-syn accumulation. Primary mice mesencephalic neurons treated with LPS. (a) a-syn oligomers. (n = 3; *p < 0.05, relatively to untreated mesencephalic neurons). (b) Representative immunoblot of a-syn oligomeric content in the mitochondria of mesencephalic neurons. (c) Densitometric analysis of mitochondrial a-syn oligomers. CT and PD cybrids exposed to LPS. (d) Representative immunoblot of a-syn oligomeric content. (e) Densitometric analysis of a-syn oligomers. (n = 4; *p < 0.05, relatively to untreated CT cybrids). NT2 Rho+ and Rho0 cells were treated with LPS. (f) Representative immunoblot of a-syn oligomeric content. (g) Densitometric analysis of a-syn oligomers. (n = 4–10; *p < 0.05, **p < 0.01 and ***p < 0.001, relatively to untreated NT2 Rho+).

Declaration of competing interest

The authors declare no conflicts of interest.

Data availability

Data will be made available on request.

Acknowledgements

The graphical abstract was created with BioRender at BioRender.com.

Appendix A. Supplementary data

Supplementary data to this article can be found online at https://doi.org/10.1016/j.redox.2023.102714.

References

[1] D.J. Surmeier, Determinants of dopaminergic neuron loss in Parkinson's disease, FEBS J. 285 (2018) 3657–3668, https://doi.org/10.1111/febs.14607.
[2] M. Goedert, M.G. Spillantini, K. Del Tredici, H. Braak, 100 years of Lewy pathology, Nat. Rev. Neurol. 9 (2013) 13–24, https://doi.org/10.1038/nrneurol.2012.242.
[3] H.L. Roberts, D.R. Brown, Seeking a mechanism for the toxicity of oligomeric alpha-synuclein, Biomolecules 5 (2015) 282–305, https://doi.org/10.3390/biom5020282.
[4] A.H. Schapira, Mitochondrial Pathology in Parkinson's Disease, vol. 78, The Mount Sinai journal of medicine, New York, 2011, pp. 872–881, https://doi.org/10.1002/msj.20303.
[5] S.M. Cardoso, The mitochondrial cascade hypothesis for Parkinson's disease, Curr. Pharmaceut. Des. 17 (2011) 3390–3397, https://doi.org/10.2174/138161211798072508.
[6] A.B. Singleton, M.J. Farrer, V. Bonifati, The genetics of Parkinson's disease: progress and therapeutic implications, Mov. Disord. 28 (2013) 14–23, https://doi.org/10.1002/mds.25249 ([doi]).
[7] A. Beilina, M.R. Cookson, Genes associated with Parkinson's disease: regulation of autophagy and beyond, J. Neurochem. 139 (Suppl 1) (2016) 91–107, https://doi.org/10.1111/jnc.13266.
[8] M. Vicario, D. Cieri, M. Brini, T. Cali, The close encounter between alpha-synuclein and mitochondria, Front. Neurosci. 12 (2018) 388, https://doi.org/10.3389/fnins.2018.00388.
[9] M.E. Johnson, B. Stecher, V. Labrie, L. Brundin, P. Brundin, Triggers, facilitators, and aggravators: redefining Parkinson's disease pathogenesis, Trends Neurosci. 42 (2019) 4–13, https://doi.org/10.1016/j.tins.2018.09.007.
[10] S.C. Park, J.C. Moon, S.Y. Shin, H. Son, Y.J. Jung, N.H. Kim, Y.M. Kim, M.K. Jang, J.R. Lee, Functional characterization of alpha-synuclein protein with antimicrobial activity, Biochem. Biophys. Res. Commun. 478 (2016) 924–928, https://doi.org/10.1016/j.bbrc.2016.08.052.
[11] S.T. Ferreira, J.R. Clarke, T.R. Bomfim, F.G. De Felice, Inflammation, defective insulin signaling, and neuronal dysfunction in Alzheimer's disease, Alzheimer's Dementia : the journal of the Alzheimer's Association 10 (2014) S76–S83, https://doi.org/10.1016/j.jalz.2013.12.010.
[12] D.F. Silva, E. Candeias, A.R. Esteves, J.D. Magalhaes, I.L. Ferreira, D. Nunes-Costa, A.C. Rego, N. Empadinhas, S.M. Cardoso, Microbial BMAA elicits mitochondrial dysfunction, innate immunity activation, and Alzheimer's disease features in cortical neurons, J. Neuroinflammation 17 (2020) 332, https://doi.org/10.1186/s12974-020-02004-y.
[13] A.R. Esteves, M.F. Munoz-Pinto, D. Nunes-Costa, E. Candeias, D.F. Silva, J. D. Magalhaes, A.R. Pereira-Santos, I.L. Ferreira, S. Alarico, I. Tiago, et al., Footprints of a microbial toxin from the gut microbiome to mesencephalic mitochondria, Gut 72 (2023) 73–89, https://doi.org/10.1136/gutjnl-2021-326023.
[14] H.Y. Liu, C.Y. Chen, Y.P. Hsueh, Innate immune responses regulate morphogenesis and degeneration: roles of Toll-like receptors and Sarm1 in neurons, Neurosci. Bull. 30 (2014) 645–654, https://doi.org/10.1007/s12264-014-1445-5.
[15] I. Morales, L. Guzman-Martinez, C. Cerda-Troncoso, G.A. Farias, R.B. Maccioni, Neuroinflammation in the pathogenesis of Alzheimer's disease. A rational framework for the search of novel therapeutic approaches, Front. Cell. Neurosci. 8 (2014) 112, https://doi.org/10.3389/fncel.2014.00112.
[16] O. Kepp, L. Galluzzi, G. Kroemer, Mitochondrial control of the NLRP3 inflammasome, Nat. Immunol. 12 (2011) 199–200, https://doi.org/10.1038/ni0311-199.
[17] A.R. Esteves, J. Lu, M. Rodova, I. Onyango, E. Lezi, R. Dubinsky, K.E. Lyons, R. Pahwa, J.M. Burns, S.M. Cardoso, et al., Mitochondrial respiration and respiration-associated proteins in cell lines created through Parkinson's subject mitochondrial transfer, J. Neurochem. 113 (2010) 674–682, https://doi.org/10.1111/j.1471-4159.2010.06631.x.
[18] A.R. Esteves, A.F. Domingues, I.L. Ferreira, C. Januario, R.H. Swerdlow, C. R. Oliveira, S.M. Cardoso, Mitochondrial function in Parkinson's disease cybrids containing an nt2 neuron-like nuclear background, Mitochondrion 8 (2008) 219–228, https://doi.org/10.1016/j.mito.2008.03.004.
[19] B.C. Dickinson, V.S. Lin, C.J. Chang, Preparation and use of MitoPY1 for imaging hydrogen peroxide in mitochondria of live cells, Nat. Protoc. 8 (2013) 1249–1259, https://doi.org/10.1038/nprot.2013.064.
[20] A.R. Esteves, M. G-Fernandes, D. Santos, C. Januario, S.M. Cardoso, The upshot of LRRK2 inhibition to Parkinson's disease paradigm, Mol. Neurobiol. 52 (2015) 1804–1820, https://doi.org/10.1007/s12035-014-8980-6.
[21] A.R. Esteves, I. Gozes, S.M. Cardoso, The rescue of microtubule-dependent traffic recovers mitochondrial function in Parkinson's disease, Biochim. Biophys. Acta 1842 (2014) 7–21, https://doi.org/10.1016/j.bbadis.2013.10.003.
[22] A.J. Valente, L.A. Maddalena, E.L. Robb, F. Moradi, J.A. Stuart, A simple ImageJ macro tool for analyzing mitochondrial network morphology in mammalian cell culture, Acta Histochem. 119 (2017) 315–326, https://doi.org/10.1016/j.acthis.2017.03.001.
[23] R. Hunter, U. Ojha, S. Bhurtel, G. Bing, D.Y. Choi, Lipopolysaccharide-induced functional and structural injury of the mitochondria in the nigrostriatal pathway, Neurosci. Res. 114 (2017) 62–69, https://doi.org/10.1016/j.neures.2016.09.007.
[24] A.F. Domingues, D.M. Arduino, A.R. Esteves, R.H. Swerdlow, C.R. Oliveira, S. M. Cardoso, Mitochondria and ubiquitin-proteasomal system interplay: relevance to Parkinson's disease, Free Radic. Biol. Med. 45 (2008) 820–825, https://doi.org/10.1016/j.freeradbiomed.2008.06.007.
[25] D.R. Binder, W.H. Dunn Jr., R.H. Swerdlow, Molecular characterization of mtDNA depleted and repleted NT2 cell lines, Mitochondrion 5 (2005) 255–265, https://doi.org/10.1016/j.mito.2005.04.003.
[26] C. Hu, Y. Huang, L. Li, Drp1-Dependent mitochondrial fission plays critical roles in physiological and pathological progresses in mammals, Int. J. Mol. Sci. 18 (2017), https://doi.org/10.3390/ijms18010144.
[27] G. Paradies, V. Paradies, F.M. Ruggiero, G. Petrosillo, Role of cardiolipin in mitochondrial function and dynamics in health and disease: molecular and pharmacological aspects, Cells (2019) 8, https://doi.org/10.3390/cells8070728.
[28] M. Garg, S. Johri, K. Chakraborty, Immunomodulatory role of mitochondrial DAMPs: a missing link in pathology? FEBS J. (2022) https://doi.org/10.1111/febs.16563.
[29] F. Peri, M. Piazza, Therapeutic targeting of innate immunity with Toll-like receptor 4 (TLR4) antagonists, Biotechnol. Adv. 30 (2012) 251–260, https://doi.org/10.1016/j.biotechadv.2011.05.014.
[30] Y. Chen, J. Lin, Y. Zhao, X. Ma, H. Yi, Toll-like receptor 3 (TLR3) regulation mechanisms and roles in antiviral innate immune responses, J. Zhejiang Univ. - Sci. B 22 (2021) 609–632, https://doi.org/10.1631/jzus.B2000808.
[31] O.W. Wan, K.K. Chung, The role of alpha-synuclein oligomerization and aggregation in cellular and animal models of Parkinson's disease, PLoS One 7 (2012), e38545, https://doi.org/10.1371/journal.pone.0038545.
[32] H. Guo, J.B. Callaway, J.P. Ting, Inflammasomes: mechanism of action, role in disease, and therapeutics, Nat. Med. 21 (2015) 677–687, https://doi.org/10.1038/nm.3893.
[33] S. Nair, K.S. Sobotka, P. Joshi, P. Gressens, B. Fleiss, C. Thornton, C. Mallard, H. Hagberg, Lipopolysaccharide-induced alteration of mitochondrial morphology induces a metabolic shift in microglia modulating the inflammatory response in vitro and in vivo, Glia 67 (2019) 1047–1061, https://doi.org/10.1002/glia.23587.
[34] J. Park, J.S. Min, B. Kim, U.B. Chae, J.W. Yun, M.S. Choi, I.K. Kong, K.T. Chang, D. S. Lee, Mitochondrial ROS govern the LPS-induced pro-inflammatory response in microglia cells by regulating MAPK and NF-kappaB pathways, Neurosci. Lett. 584 (2015) 191–196, https://doi.org/10.1016/j.neulet.2014.10.016.
[35] Y. Wang, X. Mao, H. Chen, J. Feng, M. Yan, Y. Wang, Y. Yu, Dexmedetomidine alleviates LPS-induced apoptosis and inflammation in macrophages by eliminating damaged mitochondria via PINK1 mediated mitophagy, Int. Immunopharm. 73 (2019) 471–481, https://doi.org/10.1016/j.intimp.2019.05.027.
[36] R. Kapetanovic, S.F. Afroz, D. Ramnath, G.M. Lawrence, T. Okada, J.E. Curson, J. de Bruin, D.P. Fairlie, K. Schroder, J.C. St John, et al., Lipopolysaccharide promotes Drp1-dependent mitochondrial fission and associated inflammatory responses in macrophages, Immunol. Cell Biol. 98 (2020) 528–539, https://doi.org/10.1111/imcb.12363.
[37] M. Harland, S. Torres, J. Liu, X. Wang, Neuronal mitochondria modulation of LPS-induced neuroinflammation, J. Neurosci. 40 (2020) 1756–1765, https://doi.org/10.1523/JNEUROSCI.2324-19.2020.
[38] R.L. Hunter, N. Dragicevic, K. Seifert, D.Y. Choi, M. Liu, H.C. Kim, W.A. Cass, P. G. Sullivan, G. Bing, Inflammation induces mitochondrial dysfunction and dopaminergic neurodegeneration in the nigrostriatal system, J. Neurochem. 100 (2007) 1375–1386, https://doi.org/10.1111/j.1471-4159.2006.04327.x.
[39] T. Dainichi, K. Kabashima, Ivanov, II, and Goto Y., editorial: regulation of immunity by non-immune cells, Front. Immunol. 12 (2021), 770847, https://doi.org/10.3389/fimmu.2021.770847.
[40] K. Vijay, Toll-like receptors in immunity and inflammatory diseases: past, present, and future, Int. Immunopharm. 59 (2018) 391–412, https://doi.org/10.1016/j.intimp.2018.03.002.
[41] M. Pizzuto, P. Pelegrin, Cardiolipin in immune signaling and cell death, Trends Cell Biol. 30 (2020) 892–903, https://doi.org/10.1016/j.tcb.2020.09.004.
[42] Y. He, H. Hara, G. Nunez, Mechanism and regulation of NLRP3 inflammasome activation, Trends Biochem. Sci. 41 (2016) 1012–1021, https://doi.org/10.1016/j.tibs.2016.09.002.
[43] S.S. Iyer, Q. He, J.R. Janczy, E.I. Elliott, Z. Zhong, A.K. Olivier, J.J. Sadler, V. Knepper-Adrian, R. Han, L. Qiao, et al., Mitochondrial cardiolipin is required for

Nlrp3 inflammasome activation, Immunity 39 (2013) 311–323, https://doi.org/10.1016/j.immuni.2013.08.001.
[44] Y. Han, X. Xu, C. Tang, P. Gao, X. Chen, X. Xiong, M. Yang, S. Yang, X. Zhu, S. Yuan, et al., Corrigendum to 'Reactive oxygen species promote tubular injury in diabetic nephropathy: the role of the mitochondrial ros-txnip-nlrp3 biological axis', Redox Biol. 16 (2018) 32–46, https://doi.org/10.1016/j.redox.2019.101216. Redox Biol, 24 (2019) 101216.
[45] A.R. Esteves, D.M. Arduino, D.F. Silva, S.D. Viana, F.C. Pereira, S.M. Cardoso, Mitochondrial metabolism regulates microtubule acetylome and autophagy trough Sirtuin-2: impact for Parkinson's disease, Mol. Neurobiol. 55 (2018) 1440–1462, https://doi.org/10.1007/s12035-017-0420-y.
[46] X. Ye, M. Zhu, X. Che, H. Wang, X.J. Liang, C. Wu, X. Xue, J. Yang, Lipopolysaccharide induces neuroinflammation in microglia by activating the MTOR pathway and downregulating Vps34 to inhibit autophagosome formation, J. Neuroinflammation 17 (2020) 18, https://doi.org/10.1186/s12974-019-1644-8.
[47] T. Ali, S.U. Rahman, Q. Hao, W. Li, Z. Liu, F. Ali Shah, I. Murtaza, Z. Zhang, X. Yang, G. Liu, et al., Melatonin prevents neuroinflammation and relieves depression by attenuating autophagy impairment through FOXO3a regulation, J. Pineal Res. 69 (2020), e12667, https://doi.org/10.1111/jpi.12667.
[48] A. Francois, F. Terro, N. Quellard, B. Fernandez, D. Chassaing, T. Janet, A. Rioux Bilan, M. Paccalin, G. Page, Impairment of autophagy in the central nervous system during lipopolysaccharide-induced inflammatory stress in mice, Mol. Brain 7 (2014) 56, https://doi.org/10.1186/s13041-014-0056-z.
[49] H. Yuan, C.N. Perry, C. Huang, E. Iwai-Kanai, R.S. Carreira, C.C. Glembotski, R. A. Gottlieb, LPS-induced autophagy is mediated by oxidative signaling in cardiomyocytes and is associated with cytoprotection, Am. J. Physiol. Heart Circ. Physiol. 296 (2009) H470–H479, https://doi.org/10.1152/ajpheart.01051.2008.
[50] J.J. Lum, R.J. DeBerardinis, C.B. Thompson, Autophagy in metazoans: cell survival in the land of plenty, Nat. Rev. Mol. Cell Biol. 6 (2005) 439–448, https://doi.org/10.1038/nrm1660.
[51] L. Yu, A. Alva, H. Su, P. Dutt, E. Freundt, S. Welsh, E.H. Baehrecke, M.J. Lenardo, Regulation of an ATG7-beclin 1 program of autophagic cell death by caspase-8, Science 304 (2004) 1500–1502, https://doi.org/10.1126/science.1096645.
[52] J.L. Webb, B. Ravikumar, J. Atkins, J.N. Skepper, D.C. Rubinsztein, Alpha-Synuclein is degraded by both autophagy and the proteasome, J. Biol. Chem. 278 (2003) 25009–25013, https://doi.org/10.1074/jbc.M300227200.
[53] A.R. Esteves, D.M. Arduino, R.H. Swerdlow, C.R. Oliveira, S.M. Cardoso, Oxidative stress involvement in alpha-synuclein oligomerization in Parkinson's disease cybrids, Antioxidants Redox Signal. 11 (2009) 439–448, https://doi.org/10.1089/ars.2008.2247.
[54] T.R. Sampson, C. Challis, N. Jain, A. Moiseyenko, M.S. Ladinsky, G.G. Shastri, T. Thron, B.D. Needham, I. Horvath, J.W. Debelius, et al., A gut bacterial amyloid promotes alpha-synuclein aggregation and motor impairment in mice, Elife 9 (2020), https://doi.org/10.7554/eLife.53111.
[55] A.S. Harms, V. Delic, A.D. Thome, N. Bryant, Z. Liu, S. Chandra, A. Jurkuvenaite, A.B. West, alpha-Synuclein fibrils recruit peripheral immune cells in the rat brain prior to neurodegeneration, Acta Neuropathol Commun 5 (2017) 85, https://doi.org/10.1186/s40478-017-0494-9.
[56] C.D. Hughes, M.L. Choi, M. Ryten, L. Hopkins, A. Drews, J.A. Botia, M. Iljina, M. Rodrigues, S.A. Gagliano, S. Gandhi, et al., Correction to: picomolar concentrations of oligomeric alpha-synuclein sensitizes TLR4 to play an initiating role in Parkinson's disease pathogenesis, Acta Neuropathol. 137 (2019) 121, https://doi.org/10.1007/s00401-018-1919-7.
[57] U. Ganguly, A. Banerjee, S.S. Chakrabarti, U. Kaur, O. Sen, R. Cappai, S. Chakrabarti, Interaction of alpha-synuclein and Parkin in iron toxicity on SH-SY5Y cells: implications in the pathogenesis of Parkinson's disease, Biochem. J. 477 (2020) 1109–1122, https://doi.org/10.1042/BCJ20190676.
[58] J.D. Magalhaes, A.R. Esteves, E. Candeias, D.F. Silva, N. Empadinhas, S. M. Cardoso, The role of bacteria-mitochondria communication in the activation of neuronal innate immunity: implications to Parkinson's disease, Int. J. Mol. Sci. 24 (2023), https://doi.org/10.3390/ijms24054339.
[59] A.J. Herrera, A. Castano, J.L. Venero, J. Cano, A. Machado, The single intranigral injection of LPS as a new model for studying the selective effects of inflammatory reactions on dopaminergic system, Neurobiol. Dis. 7 (2000) 429–447, https://doi.org/10.1006/nbdi.2000.0289.